THE STOCHASTIC DYNAMICS OF AN ARRAY OF MICRON SCALE CANTILEVERS IN VISCOUS FLUID

BY

MATTHEW T. CLARK

A thesis submitted to the Faculty of the
Virginia Polytechnic Institute and State University
in Partial Fulfillment of the Requirements for the Degree of
MASTER OF SCIENCE
in
Mechanical Engineering

Mark R. Paul, Chair
Danesh Tafti
Brian Vick

September 20, 2006
Blacksburg, Virginia

Abstract

THE STOCHASTIC DYNAMICS OF AN ARRAY OF MICRON SCALE CANTILEVERS IN VISCOUS FLUID

BY

MATTHEW T. CLARK

The stochastic dynamics of an array of closely spaced micron scale cantilevers in a viscous fluid is considered. The stochastic cantilever dynamics are due to the constant buffeting of fluid particles by Brownian motion and the dynamics of adjacent cantilevers are correlated due to long range effects of fluid dynamics. The measurement sensitivity of an experimental setup is limited by the magnitude of inherent stochastic motion. However, the magnitude of this noise can be decreased using correlated measurements allowing for improved force resolution. A correlated scheme is proposed using two atomic force microscope cantilevers for the purpose of analyzing the dynamics of single molecules in real time, a regime that is difficult to observe using current technologies. Using a recently proposed thermodynamic approach the hydrodynamic coupling of an array of cantilevers is quantified for precise experimental conditions through deterministic numerical simulations. Results are presented for an array of two readily available micron-scale cantilevers yielding the possible force sensitivity and time resolution of correlated measurements. This measurement scheme is capable of achieving a force resolution that is more than three fold more sensitive than that of a single cantilever when the two cantilevers are separated by 200nm, with a time scale on the order of tens of microseconds.

Library Rights Statement

In presenting the thesis *The Stochastic Dynamics of an Array of Micron Scale Cantilevers in Viscous Fluid* in partial fulfillment of the requirements for an advanced degree at Virginia Polytechnic Institute and State University, I agree that the Library shall make it freely available for inspection. I further agree that permission for copying as provided for by the Copyright Law of the U.S. (Title 17, U.S. Code) of this thesis for scholarly purposes may be granted by the Librarian. It is understood that any copying or publication of this thesis for financial gain shall not be allowed without my written permission.

I hereby grant permission to the VPI&SU Library to copy my thesis for scholarly purposes.

Matthew T. Clark

Date

Acknowledgments

I wish to thank the professors of Virginia Tech and especially those on my committee. In particular I wish to acknowledge many useful interactions with my advisor.

Table of Contents

List of Tables

List of Figures

Nomenclature

$\hat{}$	Denotes a parameter in the frequency domain
$'$	Denotes a stochastic variable (unless otherwise noted)
$*$	Complex conjugate
$\langle\rangle$	Ensemble average
a	Bead radius, (m)
β	Frequency parameter
C_n	Coefficient of the n^{th} cantilever mode
d	Molecule diameter, (m)
δ_s	Stokes length, (m)
E	Young's modulus, (N/m^2)
η	Mass per unit length, (kg/m)
η_E	Error, (%)
f_0	Resonant frequency in vacuum, (Hz)
f_s	Oscillation frequency, (Hz)
F_1	Force magnitude, (N)
F_{11}	Force sensitivity for a single cantilever, (N)
F_{12}	Correlation force sensitivity for two cantilevers, (N)
$F(t)$	Force time series, (N)
F'_B	Brownian force due to thermal motion, (N)
F_f	Force due to hydrodynamic effects, (N)
$G_F(\omega)$	Power spectral density of the Brownian force
$G_{11}(\omega)$	Power spectrum of the autocorrelated stochastic oscillations
$G_{12}(\omega)$	Power spectrum of the cross-correlated stochastic oscillations
$\gamma_f(\omega)$	Fluid damping, (kg/s)
$\Gamma(\omega)$	Hydrodynamic function
h	Cantilever thickness, (m)
I	Moment of inertia, (m^4)

k	Spring stiffness constant, (N/m)
k_B	Boltzmann's constant (1.38×10^{-23} J/K)
Kn	Knudsen number
L	Cantilever length, (m)
λ	Average free path between molecular collisions, (m)
λ_i	Exponents in a simple harmonic oscillator expression
m_w	Mass of a water molecule, (kg)
m_c	Actual system mass, (kg)
m_e	Effective mass, (kg)
m_f	Fluid loaded mass, (kg)
μ	Dynamic viscosity, (kg/m s)
N_m	Number of molecules
N_{mc}	Total number of molecular collisions
n_p	Number of system oscillations
ν_f	Fluid kinematic viscosity μ/ρ_l, (m^2/s^2)
ω	Frequency, (rad/s)
ω'	Adjusted frequency of a simple harmonic oscillator, (rad/s)
ω_0	Resonant frequency in vacuum, (rad/s)
ω_f	Resonant frequency in fluid, (rad/s)
ω^*	Frequency at which the correlation is zero, (rad/s)
p	Pressure, (N/m^2)
Q	Quality number
R	Reynolds number
ρ_c	Solid density, (kg/m^3)
ρ_l	Fluid density, (kg/m^3)
s	Separation between the two cantilevers, (m)
t, t_i	Time, (s)
Δt	Time difference, (s)

t^*	Time at which the maximum velocity occurs, (s)
T	Absolute temperature, (K)
t_c	Time between molecular collisions, (s)
t_p	Time for the first cantilever oscillation, (s)
τ	Time scale for measurements, (s)
$\vec{u}$	Velocity vector, (m/s)
U_{max}	Maximum deterministic velocity, (m/s)
$\langle v^2 \rangle$	Mean-squared velocity, (m^2/s^2)
$\langle v_i^2 \rangle$	Mean-squared velocity in the i^{th} direction, (m^2/s^2)
w	Cantilever width, (m)
$x_1(t), x_2(t)$	Stochastic displacements, (m)
$\langle x^2 \rangle$	Mean-squared displacement in the x-direction, (m^2)
X_0	Initial displacement of $X_1(t)$, (m)
$X_1(t), X_2(t)$	Deterministic deflections, (m)

1 General Overview

The measurement of protein dynamics is of interest to the scientific community as a means to better understand our world. The small force and time scales at which conformational changes occur in biological entities makes this realm difficult to investigate. Indeed, current experimental techniques are incapable of performing real time measurements of the forces exerted as a biomolecule metabolyzes substrate. As a result it is necessary for different approaches to be studied in order to reach the force and temporal resolution of single molecules. Only then can the dynamics of the biological entities important to everyday life be quantified.

This thesis presents a measurement technique that overcomes the challenges involved in investigating biological entities in real time. Microscale cantilevers such as those used in atomic force microscopes will be employed in an atypical manner. Rather than applying an external driving force to generate motion, the method described here will take advantage of the inherent stochastic beam fluctuations. However, this technique alone is only enough to improve measurements to the stochastic limit. In order to delve further into the realm of biological entities correlated measurements will be used. The thermodynamic approach is applied to quantify the stochastic dynamics of the correlated technique of interest and verify its usefulness using deterministic calculations. This approach takes advantage of the relationship between the deterministic dynamics of the system returning to equilibrium and the average stochastic motion as the system fluctuates in equilibrium.

The process of quantifying stochastic dynamics will be investigated in three steps as described below.

1. *A simple example: a bead in a trap.* The first part of this thesis will describe the principles used to investigate the stochastic dynamics of physical systems. A simple example is presented where all information about the system is known, a bead in a trap submerged in a fully viscous fluid. The stochastic dynamics are derived from the deterministic system dynamics through two methods. First, the Langevin equation that describes the system is solved analytically. Then the dynamics are derived using linear response theory to apply the fluctuation-dissipation theorem to the deterministic response of the system to the removal of a step force. These two techniques are shown to be equivalent so that the very simple physical system can be described using either approach.

2. *An experimentally motivated example: an atomic force microscope in fluid.* The next portion of this thesis will build on the knowledge gained from the simple example to investigate the stochastic dynamics of a common experimental tool, an atomic force microscope in viscous fluid. In this case the interaction between the microscopic cantilever used and the surrounding fluid is complicated. Simplified models exist to account for this hydrodynamic interaction, however the dynamics of the fluid structure coupling around the ends are neglected. This motion is important if the cantilever is to be used to measure the dynamics of biological entities. As no analytical solution to the Langevin equation exists in this case, linear response theory is applied to quantify the stochastic dynamics. The deterministic response of the microscale beam in fluid is obtained from full numerical simulations.

3. *Exploration of a new biosensor: exploiting the correlated dynamics of two adjacent AFMs.* The final part of this thesis applies the thermodynamic

approach to an experimental setup of two opposing microscopic cantilevers in viscous fluid for the purpose of analyzing single molecules in real time. In the absence of any analytical expressions for the multiple cantilevers coupled by hydrodynamic effects, full numerical simulations will be used to determine the deterministic dynamics. By applying the fluctuation-dissipation theorem to these results the stochastic dynamics can be described for a system that is beyond the realm of current theory and experiments. Knowledge gained from the study in this thesis can be used by researchers to create future experiments that will be capable of analyzing biological entities in real time.

2 Introduction

Since Richard Feynman's talk "There's plenty of room at the bottom" in 1959 [22], research across science and engineering disciplines has been done on micro and nanoelectromechanical systems. Many processes important to daily life take place on ultrasmall domains. Red blood cells, for example, have diameters on the order of 10 μm. Proteins of interest as molecular motors, such as kinesin, undergo conformational changes with forces on the order of piconewtons [5]. It is therefore beneficial to investigate thoroughly the dynamics of events in this regime so that innovative and useful designs can be constructed. By understanding the underlying physics it will be possible to make better use of recent advances in the fabrication of submicron scale structures. There have been many developments for the analysis of individual molecules, see Table 1. These techniques can be used alone or in conjunction and will be compared below.

	$F_{sens}(N)$	$X_{min}(m)$
Cantilevers	$10^{-11} - 10^{-7}$	10^{-10}
Microneedles	$10^{-12} - 10^{-10}$	10^{-9}
Flow Field	$10^{-13} - 10^{-9}$	10^{-8}
Magnetic Field	$10^{-14} - 10^{-11}$	10^{-8}
Photon Field	$10^{-13} - 10^{-10}$	10^{-9}

Table 1: Force and length scales for several small scale measurement schemes [7].

The underlying method behind each of these techniques is the application of a force or torque to the protein or polymer. When a flow field is used, a molecule is attached to a small particle or bead that acts as a handle. This bead is in turn acted upon by drag due to a moving fluid, resulting in a force

that is known from Stokes drag law. This method can become complicated if the drag of the fluid on the submerged molecule becomes large compared to drag on the handle. It is also difficult to maintain an ample concentration of biological entities when the fluid flow causes them to be driven from the measurement area. It is possible to couple a fluid force with a force from a magnetic field applied to a small magnetic particle [45]. A magnetic field can also be used to apply a torque on the magnetic bead and molecule, such that the force required to unfold molecules can be investigated [47]. While very small and stable forces can be exerted with this technique, the magnitude of the force must usually be measured with some indirect method. Photon fields use the momentum change that occurs when light refracts off of objects to exert a trapping force on a handle, similar to a mechanical spring [48]. A major drawback of this scheme is the damage that can occur in biomolecules from the lasers used. Molecules can also be trapped by adsorbing one end to the tip of a microneedle or cantilever, such as those used in atomic force microscopes. The wide availability of micron scale cantilevers in a large variety of geometries makes them a good option for an improved measurement system for single molecule manipulation. Also, the wide use of atomic force microscopes (AFM) over the past decade has led to more standardized calibration techniques, and this measurement technique can be performed in water, which is beneficial when performing measurements on biological systems.

The advent of the AFM in 1986 [6] has revolutionized surface science, see Fig. 1. The inherently small spring constants of these micron scale cantilevers make it possible to achieve measurements at high frequencies as a result of the small mass of the cantilever at this scale. This is a useful regime for measuring dynamics of molecular conformational changes, which occur on length scales on the order of angstroms at frequencies on the order of 10 Hz. The van der

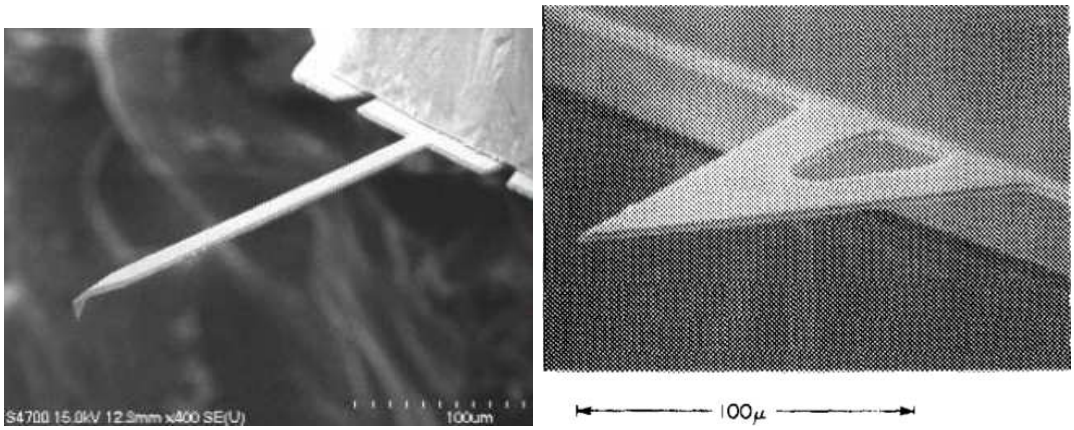

Figure 1: (left) An image of a commercially available cantilever used for atomic force microscopy [34]. A tip has been placed at the end of the cantilever in order to allow more resolved lateral measurement resolution. (right) An image of a triangular planform cantilever taken from Ref. [2].

Waals force between the cantilever tip and the sample cause the dynamics of the externally driven beam to change, and have been shown to be capable of measurements with single molecule resolution [6]. Displacements of the cantilever tip can be measured using a scanning tunneling microscope, or with an optical detection scheme [21]. The latter allows for more sensitive measurements of the deflection, even for excitation amplitudes of hundreds of angstroms [29]. It was noted that the most prevalent limitation on achieving atomic resolution with a microscopy cantilever is the difficulty in creating a sharp enough tip [29, 2]. One solution to this is the use of triangular planform cantilevers which can be constructed with near atomic accuracy to create a good point. The cantilever is then tilted in order to ensure that the interaction between the tip and sample occurs at the single molecule level [2].

In noncontact tapping mode atomic force microscopy the cantilever can be operated with a feedback signal for constant tip-sample spacing or constant force exerted between the two. The constant displacement method has been used to

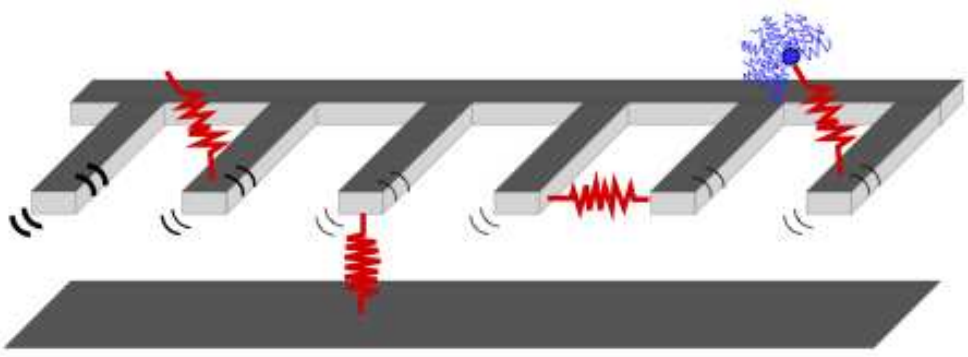

Figure 2: Application of microelectromechanical systems to the analysis of biological entities (figure from [46]). The lines around the cantilever tips indicate that the beams are undergoing stochastic fluctuations due to Brownian forces.

measure material properties of a surface at the atomic scale while simultaneously analyzing the topography of the surface. The tip-sample displacement is maintained by measuring the amplitude of oscillations in the presence of the sample and applying the difference between this and the uninhibited amplitude to the feedback loop [29]. A review of the history and principles of atomic force microscopy is given in [24].

This thesis will investigate the dynamics of AFM cantilevers undergoing random fluctuations due to a stochastic driving force rather than the external forcing commonly used for microscopy. Small scale elastic objects are constantly driven by Brownian motion, and it is this forcing that limits the resolution of a measurement scheme [8]. The scheme considered here will take advantage of this inherent stochastic motion to improve the sensitivity by using correlated measurements. A schematic of some examples of possible methods using micro and nanoscale cantilevers for biological applications is shown in Fig. 2. The spring objects in this figure are biomolecules of interest. Both the cantilevers and the molecules undergo stochastic fluctuations due to thermal motion. The cantilever is constrained at the free end by a protein tethered to a wall, a larger

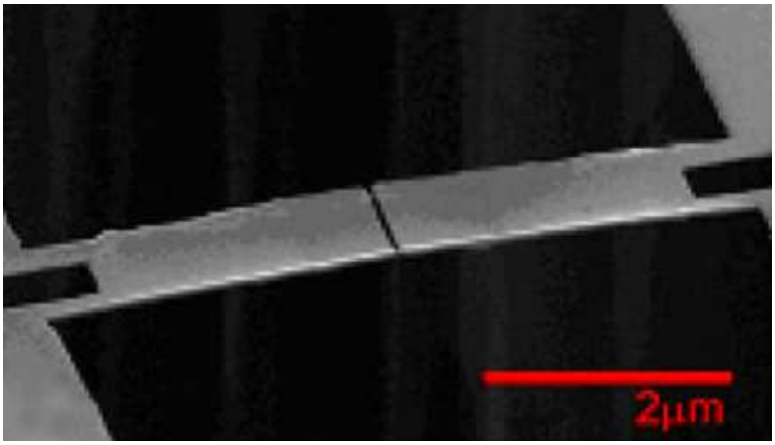

Figure 3: Nanoscale cantilevers placed with their tips 50nm apart [42].

molecule, or another cantilever. The force exerted by the protein changes the spectral dynamics of the oscillating cantilever, which can be measured experimentally and used to quantify the dynamics of the tethered molecule. An example molecule of interest is lysozyme, an egg shaped protein 5 nm in size. This protein undergoes conformational changes when metabolizing substrate on the order of 1 nm, exerting forces of 50 pN over a time span of 50 ms [39].

One of the major drawbacks in current molecular scale measurement devices is the rate at which data can be obtained. In order to investigate the dynamics of single molecules and their energy landscapes it is necessary to obtain data over a wide range of time scales [49]. Recent research in the area of micro and nanotechnology has led to the production of mechanical resonators with very high oscillation frequencies in fluid (MHz), with promise of frequencies nearing the time scale of biomolecular dynamics [41, 19]. By using surface micromachining along with lithography techniques it is possible to create complex structures with dimensions on the order of nanometers. The accuracy and repeatability of these methods must be improved such that atomically flat surfaces can be created. Structures with dimensions in this regime have extremely small masses

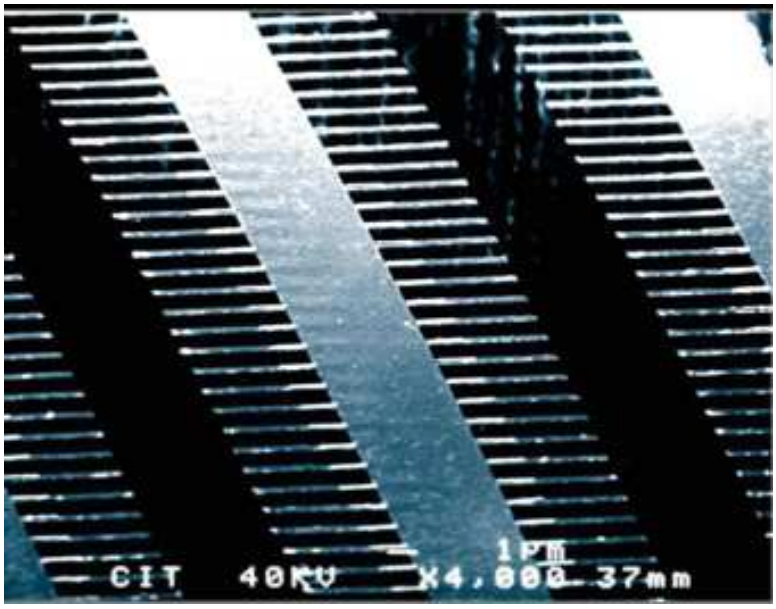

Figure 4: An array of micron sized cantilevers [42]. The motion of these beams in fluid would be coupled due to the hydrodynamic interaction.

($\sim pg$), indicating that the structure will have a high resonant frequency even with a relatively low spring constant common in submicron scale systems. This means that measurements can be taken with ever higher temporal resolution as the system mass decreases.

All macroscopic objects are constantly undergoing random fluctuations, though at a scale that is imperceptible in everyday objects. However, in the submicron regime the magnitude of these stochastic oscillations is within the realm of measurement and therefore noise inherent in experimental systems. The dependence of the root-mean-squared displacement on the inverse of stiffness (see Chapter 3) means that the magnitude of thermally induced fluctuations will increase as systems get smaller and the structures become softer. This leads to a trade-off between force and time resolution of a measurement scheme.

The stochastic dynamics of micro and nanoscale structures are complicated.

It is the random fluctuations due to thermal forcing that limits the sensitivity in experiments. Common measurement techniques rely on external driving forces to investigate molecular dynamics and therefore have resolutions limited these stochastic oscillations. The experimental method described here will take advantage of correlations to obtain improved resolution beyond the magnitude of these random fluctuations [28]. Fluctuations in a system parameter due to Brownian noise forces will be uncorrelated and not contribute. When two system parameters become coupled, the fluctuations in the parameters become correlated. Additional external forcing can be observed as a variation in the correlated system dynamics and the noise floor becomes the magnitude of the parametric coupling. A scheme where system parameters are coupled can be used to obtain measurements lower than the magnitude of thermal noise inherent in the system without effecting the temporal resolution. In order to quantify the stochastic dynamics of coupled objects it is necessary to understand the underlying physics behind thermally induced motion. Therefore the Brownian dynamics must be quantified so that measurement schemes can be investigated prior to construction.

The dynamics of systems in the submicron regime are often complicated further by the presence of a fluid environment. This is the case when investigating biological entities that are in aqueous solution. Fluid dissipation changes the spectral dynamics of an oscillating structure and therefore must be investigated. In addition, the presence of solid objects in the fluid surrounding an object affects the power spectrum of thermally induced oscillations. A detailed study for the precise conditions of experiment is necessary to fully describe the motion of a microscale object in fluid.

In an experimental scheme for the analysis of single molecules proteins are adsorbed onto a microscopic tip on the distal end of the cantilever [23]. As the

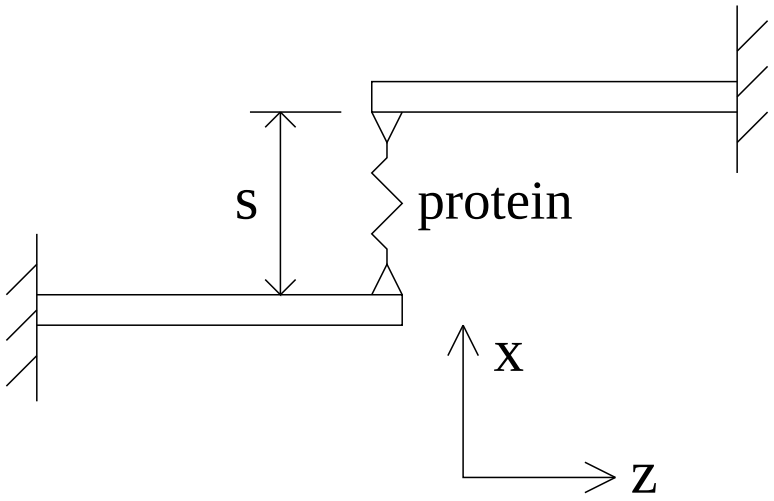

Figure 5: A schematic of the experimental method described in the text, not to scale. A protein is tethered to the tips of two cantilevers that are separated by s. The cantilevers are 2μm thick, probe tips are available in heights from 500nm to 10μm, and the protein is approximately $50\mathring{A}$.

biomolecule undergoes conformational changes, the size of the molecule changes and causes a force to be exerted on the beam. This change can be measured by analyzing the shift in the spectral dynamics of the oscillating system. In the correlated measurement scheme discussed here two cantilevers are placed close to each other in fluid and a biomolecule will tethered between the two tips as shown in Fig. 5. The shift in the thermally induced oscillations in the two beams due to the presence of the protein will be used to quantify the molecular dynamics. It is common for these small scale systems to be created in large arrays or near some other solid object, see Fig. 4. For this reason it is necessary to study the long range effects of fluid motion caused by micron scale objects. The coupled motion that results from small scale objects near one another in fluid has been exploited to improve measurement sensitivity for the case of two micron size beads in photon traps tethered by DNA [31]. This approach is not useful for measurement of protein dynamics as the trap relaxation time is of the

same magnitude as the metabolisys of lysozyme. In addition, the trap stiffness is $\sim 10^{-5}$N/m meaning that forces exerted by lysozyme will cause the beads to be pulled from the photon traps [39]. The use of correlated measurements has been extended to multiple nanoscale cantilevers in fluid separated by nanometers [38]. Also, the effects of a solid wall on the motion of micron sized cantilevers has been studied [16, 25]. The fluid coupling due to the stochastic motion of multiple cantilevers will be studied here to gain a better understanding of fluid coupling between submicron scale objects, see [15] for a review. Future work can build on this knowledge to investigate the dynamics of proteins at the single molecule level.

3 Quantifying the Stochastic Dynamics of Elastic Objects Immersed in Fluid

Before attempting to quantify the stochastic dynamics of a microscopic system it is necessary to present the principles used to describe them. The purpose of this chapter is to present a brief overview of a recently proposed thermodynamic approach capable of quantifying the dynamics of a physical system through the use of statistical mechanics and the fluctuation-dissipation theorem. Using this tool it will be possible to quantify the stochastic motion of any experimentally relevant system from deterministic calculations. The use of this approach will be covered in subsequent chapters.

The first approach to quantifying the underlying physics of micron scale objects that many people consider would be to model the system with a full molecular dynamics simulation [11]. This would involve calculating momenta for each molecule in the solid and fluid at intervals the length of time between molecular collisions. Imagine an atomistic approach that resolves every collision that occurs. For a $1000\mu\text{m}^3$ volume of water having a molecular diameter $d \approx 3\mathring{A}$, the molecular dynamics must be solved for $N_m \sim 10^{14}$ molecules. This estimate assumes spherical molecules packed into a cube with a packing factor of 0.6 [50]. A rough estimate of the time between collisions can be obtained from the equipartition theorem of energy. The equipartition theorem of energy states that the energy in each quadratic mode and in each degree of freedom has the same amount of thermal energy and is equal to $k_B T/2$, where T is the absolute temperature and $k_B = 1.38 \times 10^{-23}\text{J/K}$ is Boltzmann's constant, which relates the amount of energy in a molecule to the temperature of the system. The average kinetic energy for a single molecule is equated to this value to obtain,

$$\frac{1}{2} m_w \left\langle v^2 \right\rangle = \frac{3}{2} k_B T \tag{1}$$

Here $m_w \approx 1$zg (1 zeptogram $= 10^{-21}$grams) is the mass of a water molecule and $\langle v^2 \rangle = \langle v_x^2 \rangle + \langle v_y^2 \rangle + \langle v_z^2 \rangle$ is the magnitude of the mean-squared absolute velocity for a water molecule. The mean-squared velocity of a molecule in each direction will be the same, i.e. $\langle v^2 \rangle = 3 \langle v_x^2 \rangle$. The time between molecular collisions t_c can then be obtained from the root-mean-squared absolute velocity $\langle v^2 \rangle^{1/2}$ and mean free path between collisions λ using $t_c = \lambda / \langle v^2 \rangle^{1/2}$. Using the diameter of a water molecule as the mean free path between collisions, $\lambda \approx 3\mathring{A}$, the time between collisions for each molecule is $t_c \approx 2.7$ps. This agrees with commonly used molecular dynamics time steps [11]. In order to obtain good statistics for the probability functions describing the stochastic motion of a system the solution must be obtained for many initial conditions, or for a very long time so that all states of the equilibrium system are represented. Consider a system oscillating at f_s =25kHz that will be allowed to undergo n_p =1000 oscillations. For this case each molecule will experience $n_c = n_p/(f_s t_c) = 4 \times 10^{10}$ collisions during the time the system will oscillate. This means that a total of $N_{mc} = n_c N_m = 4 \times 10^{24}$ molecular collisions must be calculated. Assuming it takes one clock cycle to calculate the dynamics for a single collision, it would take a 1GHz processor 1×10^8 years to complete these calculations!

Instead the dynamics of both fluid and structure can be investigated by taking advantage of thermal equilibrium, meaning that ensemble averages of the system dynamics can be quantified. A system in thermal equilibrium can be described using statistical mechanics. All micro and macroscopic objects are in constant thermal motion, however the motion is not visible in macroscopic objects. Molecules at a finite temperature are in constant thermal motion resulting in random fluctuations in particle position. For microscale systems, these microscopic perturbations are the noise that limits the resolution of measurements.

When a system is in thermal equilibrium the average fluctuations in particle

position can be quantified. The average potential energy in the x-direction of a system with stiffness k is equated to the amount of thermal in each quadratic energy mode in one direction to obtain,

$$\frac{1}{2}k\left\langle x^2\right\rangle = \frac{1}{2}k_B T. \tag{2}$$

Here $\langle x^2\rangle^{1/2}$ is the root mean squared system displacement in the x-direction. The angle brackets $\langle\rangle$ represent an ensemble average over all possible initial conditions. Equation (2) is often used in experiment to obtain the spring constant for a system [18]. The quantity on the right hand side is a known constant and the root mean squared displacement can be measured directly. It should be noted that this average is independent of the viscosity of the surrounding fluid.

3.1 Fluctuation-Dissipation Theorem

The fluctuation dissipation theorem [10, 9, 13] can be used to describe the stochastic dynamics of a microscale system. Submerged objects in thermal equilibrium are constantly bombarded by fluid molecules. If the system is perturbed from equilibrium and allowed to settle it will approach a meta-stable equilibrium. When the perturbation is removed the system will relax back to its original thermal equilibrium. The dynamics of the system as it relaxes from a macroscopic perturbation are directly related to the regression of microscopic fluctuations (see Onsager regression hypothesis [35]). The power spectrum of Brownian noise force is given by G_F. For an elastic object in fluid the fluctuation-dissipation theorem states that the stochastic fluctuations of the system in equilibrium are directly related to the damping γ_f due to interactions between the fluid and solid [9]. In other words, when the system is returning to equilibrium from a small but macroscopic perturbation it is damped by the action of fluid molecules. The stochastic fluctuations of a system in equilibrium

are known to be related to the system dissipation by,

$$G_F(\omega) = 4k_B T \gamma_F(\omega). \tag{3}$$

The most important aspect of this equation is that the left hand side is a stochastic quantity, whereas the right side is deterministic. Dynamics of deterministic systems can be specified precisely by previous dynamics, while stochastic dynamics can only be described by probability functions. The stochastic dynamics of a system in equilibrium can be derived from deterministic calculations of the macroscopic system dynamics. It is of note that, except in very simple cases (see Chapter 3) the stochastic forcing has a frequency dependence and therefore the thermal forcing is not white noise.

The fluctuation-dissipation theorem can also be expressed using linear response theory [13, 38, 37]. This approach is useful when the interaction between a system and the surrounding fluid is difficult to describe. When fluctuations of a system are kept small enough the dynamical system response is linearly coupled to the perturbation. The special case is considered where a step force $F(t)$ is applied in the distant past and removed at zero time,

$$F(t) = \begin{cases} F_1 & \text{for } t < 0 \\ 0 & \text{for } t \geq 0. \end{cases} \tag{4}$$

This allows the system to adjust to the perturbation and non-equilibrium fluctuations to decay. The relaxation of the system back to equilibrium after this macroscopic disturbance can be used in the fluctuation-dissipation theorem to obtain the auto and cross-correlation of the stochastic system oscillations [38, 37]. The autocorrelation quantifies the correlation between stochastic oscillations and a spontaneous microscopic fluctuation separated by some time span,

$$\langle x_1(0) x_1(t) \rangle = \frac{k_B T}{X_0 k} X_1(t). \tag{5}$$

Here $F_1 = X_0 k$, X_0 is the initial deflection of $X_1(t)$ and $X_1(t)$ is the dynamical response of the deterministic system to the perturbation. The uppercase $X(t)$ are the deterministic deflections and the small $x(t)$ are the stochastic fluctuations of the object. Deterministic quantities are derived by neglecting the influence of stochastic variables in the system. The Onsager regression principle [35] states that the dynamics of the deterministic and stochastic representation of a system are inherently linked, as shown by the relationship for the fluctuation-dissipation theorem given above in Eq. (3).

The left side of Eq. (5) is the autocorrelation of equilibrium displacements and the right side is the deterministic deflection scaled to ensure that the energy of stochastic oscillations in the x-direction is equivalent to the molecular energy at thermal equilibrium. The autocorrelation quantifies the average stochastic dynamics over all possible states of the system in equilibrium. Also, the autocorrelation depends only on the time difference Δt, for example if $t_3 = t_2 + \Delta\text{t} = t_1 + 2\Delta\text{t}$ the correlations $\langle x_1(t_1)x_1(t_2)\rangle = \langle x_1(t_2)x_1(t_3)\rangle$.

When a second dynamical variable x_2 is considered the correlations between stochastic oscillations in x_2 and a spontaneous microscopic fluctuations in x_1 separated by some time span are quantified by the cross-correlation,

$$\langle x_1(0)x_2(t)\rangle \quad = \quad \frac{k_B T}{X_0 k} X_2(t). \tag{6}$$

Any coupling that occurs between x_1 and x_2 will show up as correlated dynamics in the cross-correlation. X_2 is a dynamical variable of the system that couples to the fluctuations X_1. The coupled motion X_2 is multiplied by the same scaling factor as the autocorrelation in order to satisfy equipartition.

From the auto and cross-correlations it is possible to determine the noise spectrum for thermally induced oscillations from the cosine Fourier transform [38, 37]. The power spectra for the auto and cross correlated stochastic

oscillations are

$$G_{11}(\omega) = 4\int_0^\infty \langle x_1(0)x_1(t)\rangle \cos(\omega t)dt, \quad (7)$$

$$G_{12}(\omega) = 4\int_0^\infty \langle x_1(0)x_2(t)\rangle \cos(\omega t)dt, \quad (8)$$

and have been derived in Ref. [37]. These quantities are precisely those that would be measured in experiment for two objects undergoing stochastic fluctuations [29, 18]. The power spectrum of stochastic oscillations quantifies the energy of the response in a frequency range.

4 A Simple Example: Submerged Bead in a Trap

The previous section presented a thermodynamic approach that can be used to quantify the stochastic dynamics of physical systems. In this chapter the thermodynamic approach is applied to a simple case so that the method can be described in detail. The two expressions of the fluctuation-dissipation theorem presented will be applied to this simple case and will be shown to be equivalent. Later chapters will quantify the dynamics of more complex systems using the same approach shown here.

The dynamics of a cantilever in fluid are complex and require simplified models or numerical simulations to describe in full. Instead, a simple example is explored in this section where the interaction between the fluid and solid can be described analytically. Specifically, the fully viscous regime is examined where the Reynolds number and frequency parameter are $R = \beta = 0$ (see Eq. (37) and (38)). In this regime the fluid force on simple objects can be described using Stokes law and the analysis is greatly simplified [36].

A schematic of the system of interest is shown in Fig. 6. The spherical bead has a radius $a = 1\mu$m and is composed of silicon ($\rho_c = 2320$ kg/m^3) and attached to a spring of stiffness $k = 1$N/m. The actual mass of the sphere is $m_c = 4\pi a^3/3 = 9.76 \times 10^{-15}$kg, and in this case where a lumped mass is considered the effective mass reduces to $m_e = k/\omega_0^2 = m$. The stochastic motion of the bead is described by the Langevin equation,

$$m_e\ddot{x} + kx = F_f + F_B'. \tag{9}$$

Here x is the stochastic motion of the mass, F_B' is the thermal forcing, and F_f is the force exerted by the fluid on the object. The random force F_B' due to thermal motion as a function of time is a very complicated function and must be quantified. The prime on F_B' is notation to emphasize that the force is a

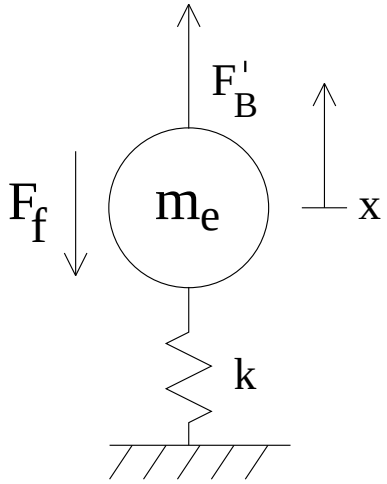

Figure 6: A bead with radius $a = 1\mu$m is attached to a spring of stiffness $k = 1$N/m and submerged in water ($\mu = 8.55 \times 10^{-4}$ kg/m s). F_f is the force of fluid damping on the bead as it moves and F'_B is the stochastic force on the bead due to Brownian motion.

random variable. For the fully viscous regime the force of fluid damping on a sphere is known from Stokes drag law [36] to be,

$$F_f = \gamma_f \dot{x} = -6\pi\mu a\dot{x}. \tag{10}$$

The force that the fluid exerts of the spherical bead is directly related to its velocity and acts to oppose the motion. The fluid dissipation γ_f is a constant and the spectral density of the Brownian force is given directly from Eq. (3),

$$G_F(\omega) = 24\pi k_B T a\mu. \tag{11}$$

In the case of a sphere in the low Reynolds number regime the thermal forcing is not frequency dependent, meaning it is white noise under these conditions. The power spectrum of Brownian noise force has now been quantified and the solution to the stochastic equation of motion Eq. (9) can be obtained. The

equation will be solved in the Fourier space using the convention,

$$x(t) = \frac{1}{2\pi}\int_{-\infty}^{\infty} \hat{x}(\omega)e^{-i\omega t}d\omega, \tag{12}$$

$$\hat{x}(\omega) = \int_{-\infty}^{\infty} x(t)e^{i\omega t}dt. \tag{13}$$

After substituting Eq. (10) into Eq. (9), calculating the Fourier Transform using Eq. (13), and solving the equation for $\hat{x}(\omega)$ the result is,

$$\hat{x}(\omega) = \frac{\hat{F'}_B}{(k - m_e\omega^2) + i(\omega\gamma_f)}. \tag{14}$$

The power spectrum of the stochastic bead fluctuations can be obtained by multiplying Eq. (14) by the complex conjugate to obtain,

$$|\hat{x}(\omega)|^2 = \frac{\hat{F'}_B\hat{F'}^*_B}{(k - m_e\omega^2)^2 + (\gamma_f\omega)^2}, \tag{15}$$

where $*$ denotes a complex conjugate. The left side of the equation is the noise spectrum of thermally induced oscillations $G_{11}(\omega)$ and $G_F = \hat{F'}_B\hat{F'}^*_B$ is the spectral density of thermal forcing as obtained from the fluctuation dissipation theorem, Eq. (11). These two quantities can then be related by,

$$G_{11}(\omega) = \frac{G_F}{(k - m_e\omega^2)^2 + (\gamma_f\omega)^2} = \frac{4k_BT\gamma_f}{(k - m_e\omega^2)^2 + (\gamma_f\omega)^2}. \tag{16}$$

The factor multiplying the G_F is the system susceptibility, the response of the system to a force impulse.

4.1 Solution using Linear Response Theory

This result can also be found by applying linear response theory to obtain the auto-correlation of stochastic oscillations $\langle x_1(0)x_1(t)\rangle$ using Eq. (5), and then the spectral density of stochastic bead oscillations due to thermal forcing $G_{11}(\omega)$ from Eq. (7). In this lumped mass case the deterministic bead motion is given by the simple harmonic oscillator (SHO) response to the removal of a step force (see Eq. (4)). While this representation of the system is not physical, the

underlying physics are the same as those for the actual stochastic system [35]. The bead deflection can then be described by the solution to the equations,

$$m_e\ddot{X}_1 + \gamma_f\dot{X}_1 + kX_1 = 0, \tag{17}$$

$$X_1(0) = X_0 = \frac{F_1}{k}, \tag{18}$$

$$\dot{X}_1(0) = 0. \tag{19}$$

The root-mean-squared displacement of the trapped bead system can be obtained from equipartition of energy, Eq. (2), to be 0.6 $\mathring{A}$. For reference, the ratio of the root-mean-squared bead displacement to its radius is,

$$\frac{\langle x^2\rangle^{1/2}}{a} = 6.4 \times 10^{-5}. \tag{20}$$

Due to the linear nature of the governing equations a solution for the displacement of the bead as a function of time can be obtained analytically, and the solution is,

$$X_1(t) = Ae^{\lambda_1 t} + Be^{\lambda_2 t}. \tag{21}$$

Here A and B are arbitrary constants that will be obtained when the initial conditions are applied to the solution. The exponents λ_1 and λ_2 are defined as,

$$\lambda_1 = \frac{1}{\omega_f}\left(-\frac{1}{2Q} + \sqrt{\frac{1}{4Q^2-1}}\right), \tag{22}$$

$$\lambda_2 = \frac{1}{\omega_f}\left(-\frac{1}{2Q} - \sqrt{\frac{1}{4Q^2-1}}\right). \tag{23}$$

The parameters shown in these equations are the quality number Q and the damped oscillation frequency ω_f for the bead. The quality of an oscillator represents the amount of the system's total energy that is dissipated in each oscillation and the damped frequency is the resonant frequency of the cantilever in viscous fluid. The two are defined from the trapped bead parameters as,

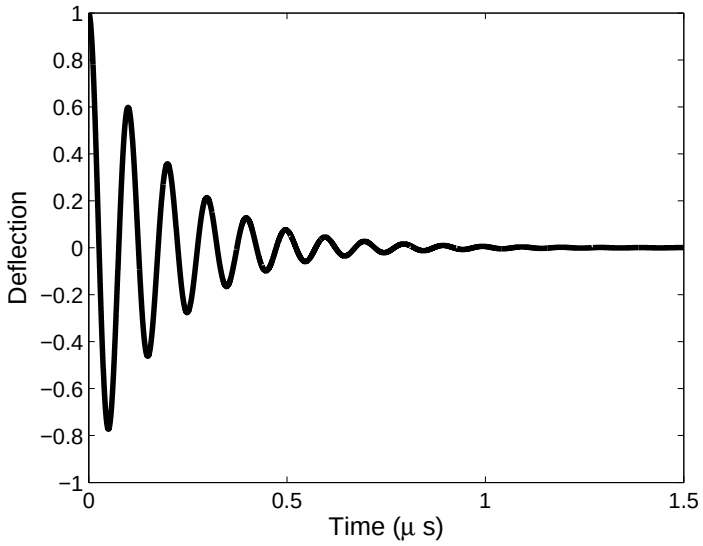

Figure 7: Normalized deterministic oscillations of the trapped bead in fluid.

$$\omega_f = \sqrt{\frac{k}{m_f}}, \tag{24}$$

$$Q = \frac{m_f \omega_f}{\gamma_f}. \tag{25}$$

For the system parameters given above the SHO variables are $Q = 6.13$ and $\omega_f = 63.5 \times 10^6$ rad/s (10.1 MHz). In Eq. (24) the fluid loaded mass m_f is the effective mass of the oscillator accounting for inertial effects of the fluid moving along with it. The assumption that R$\rightarrow$ 0 means that only viscous effects are considered, and the fluid loaded mass is equal to the effective mass, $m_f = m_e$. When the term under the radical in Eq. (22) and (23) is greater than zero the exponents are real and the system will not exhibit oscillatory behavior (overdamped case). The bounding case occurs when $Q = 1/2$ and is the critically damped case. For the case of the trapped bead described above the quality is $Q > 1/2$, therefore the system is underdamped. After applying the initial conditions the solution can be defined as in Eq. (26).

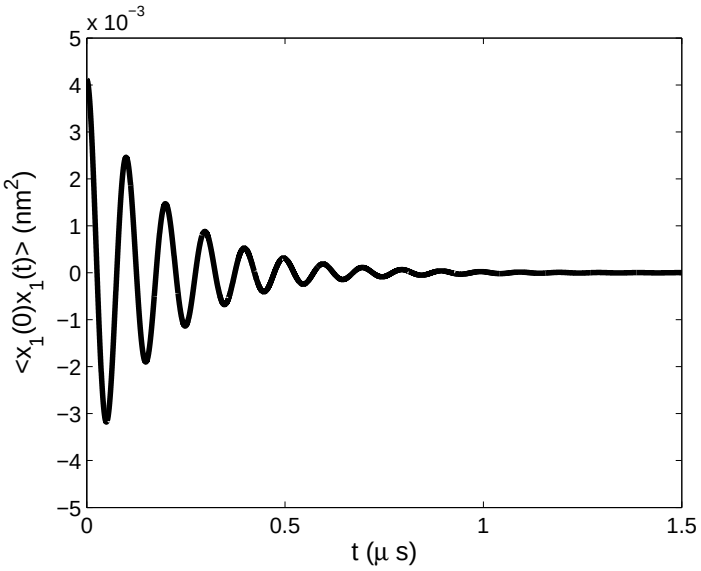

Figure 8: Autocorrelation for the trapped bead in fluid. This is the equilibrium average for all possible initial conditions and is simply the deterministic dynamics multiplied by a constant.

$$X_1(t) = X_0 e^{\frac{-\omega_f t}{2Q}} \left(\cos \omega' t + \frac{\omega_f}{2Q\omega'} \sin \omega' t \right), \tag{26}$$

$$\omega' = \omega_f \sqrt{1 - \frac{1}{4Q^2}}. \tag{27}$$

A plot of the bead deflection for the case of a step force is shown in Fig. 7. The motion of the bead is completely deterministic, that is all dynamics of the system can be described by the conditions of the system at some previous time.

4.2 Stochastic Bead Dynamics

Next the fluctuaction-dissipation theorem is applied to the deterministic bead deflection in order to obtain the autocorrelation for the stochastic fluctuations using Eq. (5). This function quantifies the correlations in the bead motion that would be detected in the physical system for any initial conditions and is shown in Fig. 8. The quantity is just the deterministic motion scaled by a constant value.

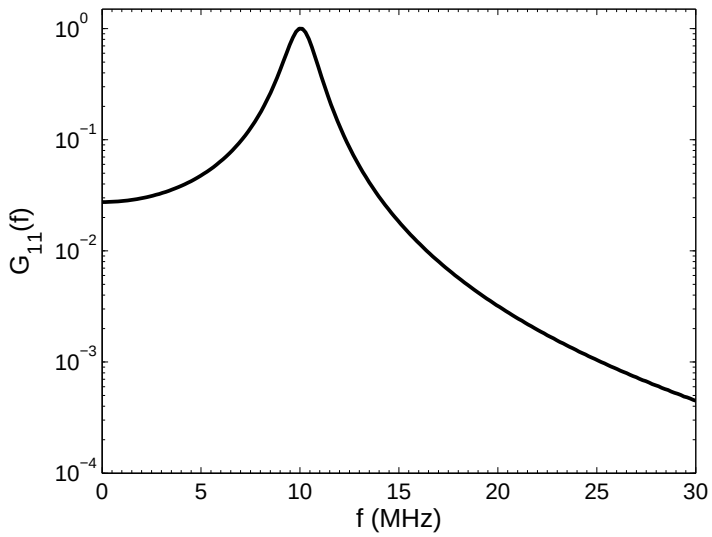

Figure 9: Normalized noise spectrum of the submerged bead in a trap, the peak occurs at $f \approx$10 MHz. $G_{11}(f)$ is shown in arbitrary units. This is the power spectrum of stochastic bead oscillations.

The value of the auto-correlation at zero time delay is approximately $\langle x^2 \rangle = 4 \times 10^{-3}$ nm^2. This corresponds to an average displacement $\langle x^2 \rangle^{1/2} = 0.63\mathring{A}$, as required by equipartition of energy. Next, the power spectrum of the auto-correlation for thermally induced oscillations $G_{11}(\omega)$ can be obtained by substituting Eq. (26) into Eq. (5) and then applying Eq. (7) to the autocorrelation. The resulting power spectrum is shown in Fig. 9. This is precisely the quantity that would be measured in an experiment. Substituting Eq. (24) and (25) into Eq. (26) and obtaining the cosine Fourier transform (using Mathematica [30]) the power spectrum of stochastic oscillations is found to be,

$$G_{11}(\omega) = \frac{4k_B T \gamma_f}{\left(k - m_e \omega^2\right)^2 + \left(\gamma_f \omega\right)^2}.$$

This is the same result that was obtained in Eq. (16), meaning that applying the fluctuation-dissipation through linear response theory is equivalent to the direct method of solving the Langevin equation. However, by taking advantage

of linear response theory it is possible to quantify stochastic dynamics when the fluid damping is difficult to describe.

5 The Deterministic Dynamics of a Cantilever in Viscous Fluid

The previous chapter presented the method for deriving the stochastic dynamics of a microscale elastic object in fluid from its deterministic motion. This same approach will be applied to describe the random motion of a submerged cantilever by analyzing the system's deterministic response to the removal of a step force. First, the mechanics of the solid beam under loading will be studied and then the dynamics of the fluid. Next the interaction between the fluid and solid will be investigated in order to describe the flow field around an oscillating cantilever. After this the correlated dynamics of two submersed AFM cantilevers will be analyzed in the same manner.

L	w	h	k	f_0	$\langle x^2 \rangle^{1/2}$
197μm	29μm	2.0μm	1.32 N/m	71.94 kHz	0.56 $\mathring{A}$

Table 2: Summary of the cantilever geometry and properties. The geometry is given by the cantilever length L, width w, and height h. The root-mean-square of the cantilever's thermally driven oscillations is given by $\langle x^2 \rangle^{1/2}$. The cantilevers are composed of silicon with density $\rho_c = 2320$ kg/m^3, and Youngs modulus E $= 1.74 \times 10^{11}$ N/m^2. The cantilevers are immersed in water with density $\rho_l = 997$ kg/m^3 and dynamic viscosity $\mu = 8.59 \times 10^{-4}$ kg/m-s.

By taking advantage of the fluid coupling between immersed objects the noise floor of a measurement can be lowered [32]. Very long and thin microscopic cantilevers in viscous fluid will be studied in the orientation shown in Fig. 10(b) as a possible experimental setup capable of achieving improved measurement resolution. The motion of the two cantilevers will be correlated through the induced fluid motion, and also due to the dynamics of a protein tethered between the two tips. The coupling due to the protein can then be used to quantify the dynamics of conformational changes or as a single molecule sensor. In order for this measurement scheme to be useful the noise due to fluid interaction must

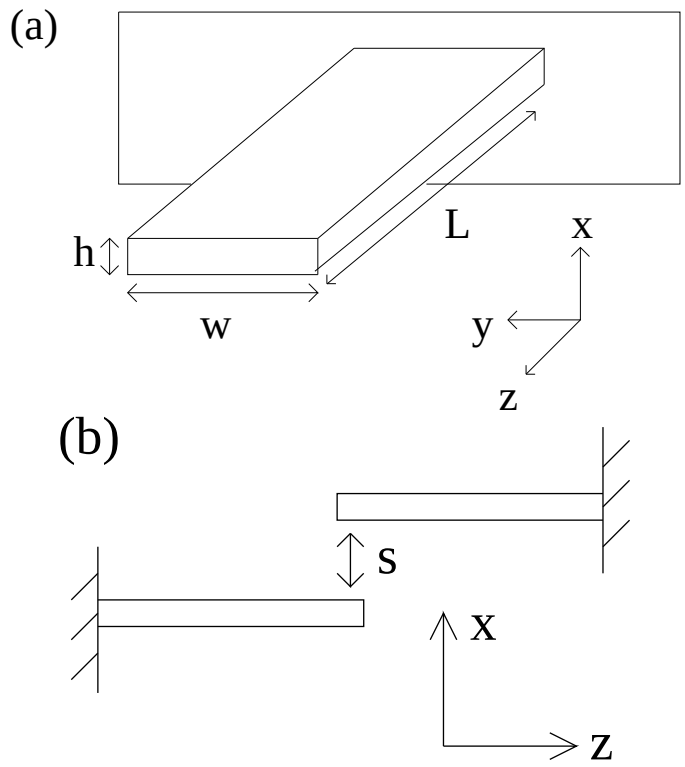

Figure 10: (a) The convention used in defining the cantilever geometry, not to scale. Actual aspect ratios are $L/h = 98.5$, $w/h = 14.5$, and $L/w = 6.8$. Specific properties of the cantilevers explored here are given in Table 2. (b) The explored configuration of two adjacent micron scale cantilevers (not drawn to scale). In the absence of a tethered biomolecule between the cantilevers their motion will be correlated due to the induced fluid motion.

be of lower magnitude than the coupling due to the biomolecule. It is first necessary to describe the dynamics of the hydrodynamic coupling between two submerged beams in order to ensure that the magnitude of this noise is smaller than that of the tethered molecule of interest.

5.1 Cantilever Dynamics in Vacuum

The physical properties of the cantilevers investigated here are shown in Table 2. The spring constant k and resonant frequency of the beam in vacuum ω_0 are calculated from the equations of beam theory [27] for a cantilevered beam

as,

$$k = \frac{3EI}{L^3}, \tag{28}$$

$$\omega_0 = 2\pi f_0 = \frac{C_1^2}{L^2}\sqrt{\frac{EI}{\eta}}. \tag{29}$$

In the above equations E is Young's modulus, $I = wh^3/12$ is the beam moment of inertia and $\eta = \rho_c wh$ is the mass per unit length. C_1 is the coefficient for the first cantilever mode and is the first solution to,

$$1 + \cos C_n \cosh C_n = 0, \tag{30}$$

where $n = 1, 2, 3, ...$ is the mode number. For the cantilevers of interest here $k = 1.32$ N/m and $\omega_0 = 452 \times 10^3$ rad/s (71.9 kHz). These parameters can also be obtained from simulations of a beam in vacuum, a simple calculation that takes a very short time to run. This is important because these results will be shown to be useful later for describing the dynamics of a cantilever under the influence of fluid dissipation [43], where the damped frequency of oscillation in fluid ω_f and the quality Q factor will be derived using the natural frequency of the beam in vacuum ω_0 and the spring constant k. Once the spring constant is known the root mean squared displacement for the cantilever in vacuum can be determined from Eq. (2) to be $\langle x^2 \rangle^{1/2} = 0.56\mathring{A}$. The magnitude of the thermally induced oscillations for the cantilever is shown in Eq. (31) with reference to the beam height,

$$\frac{\langle x^2 \rangle^{1/2}}{h} = 2.8 \times 10^{-5}. \tag{31}$$

This is the magnitude of the noise that limits the spatial resolution of measurements using a single AFM cantilever. In order to more completely describe the stochastic dynamics of microscale cantilevers the deterministic mechanics of the beam in fluid will be investigated and then the fluctuation-dissipation theorem can be applied.

5.2 Deterministic Beam Mechanics

The dynamics of the solid structure can be described by the Euler-Bernoulli beam equation, Eq. (32), a special case of the elasticity equations [27],

$$EI\frac{\partial^4 X(z,t)}{\partial z^4} + \eta\frac{\partial^2 X(z,t)}{\partial t^2} = F(z,t), \tag{32}$$

$$X(0,t) = \frac{\partial X(0,t)}{\partial z} = 0, \tag{33}$$

$$\frac{\partial^2 X(L,t)}{\partial z^2} = \frac{\partial^3 X(L,t)}{\partial z^3} = 0. \tag{34}$$

Boundary conditions are specified for the case where the beam is cantilevered. At $z = 0$ is a fixed boundary, Eq. (33), the deflection is specified as zero and the beam must have zero slope. At $z = L$, Eq. (34), is a free boundary condition, described by zero bending moment and shear. The initial configuration of the beam is fully formulated by the forcing on the beam given by the step force in Eq. (4); that is the beam starts at some initial deflection with no velocity. Fluid coupling is accounted for by the source term on the right side of the governing equation as a function of position and time. This forcing is complex and strongly dependent on the previous motion of the beam, and the fluid motion generated by the beam will cause complicated dynamics in the near field. Therefore, it is necessary to describe the fluid dynamics that will cause the forcing in this equation for both an externally forced beam and one driven by induced fluid motion.

5.3 Deterministic Fluid Dynamics

Before investigating the dynamics of the fluid it is necessary to determine which assumptions are valid in this regime. As the size of a physical system is decreased into the micron range, the validity of classical mechanics equations commonly used comes into question. At some point the size of the apparatus

reaches the order of single molecules in the surroundings and continuum mechanics no longer holds, with consequences such as the breakdown of the no slip hypothesis. Past this realm it becomes necessary to compute molecular dynamics for the surrounding fluid, a very computationally intensive process for any appreciable sized domain. The characteristic length scale for the cantilevers investigated here is the beam half width, w/2 = 14.5μm. The ratio of the mean free path between collisions for the surrounding fluid, λ, to this length scale gives the nondimensional value known as the Knudsen number, Kn. For Kn$\rightarrow$ 0 the continuum hypothesis is valid. Comparisons between experiment and theory have shown that for values Kn $\lesssim 10^{-3}$ the fluid environment can be treated as a continuous medium without introducing error [44, 26]. For the specific configuration studied here λ is the diameter of a water molecule and we find Kn = λ/L $\approx 10^{-5}$. The small magnitude of the Knudsen number leads to the assumption of continuum mechanics and no-slip boundaries in the remainder of this thesis. The continuous fluid medium surrounding the cantilevers is modeled by the nondimensionalized Navier-Stokes equations [36],

$$\beta \frac{\partial \vec{u}}{\partial t} + R\ \vec{u}\bullet\vec{\nabla}\vec{u} = -\vec{\nabla}p + \nabla^2\vec{u}, \tag{35}$$

$$\vec{\nabla}\bullet\vec{u} = 0. \tag{36}$$

Eq. (35) and (36) represent the conservation of momentum and mass equations for an incompressible fluid. The nondimensional variables R and β are the Reynolds number and frequency parameter, respectively. The Reynolds number, Eq. (37), is the ratio of convective inertia effects to viscous effects in the fluid. The frequency parameter, Eq. (38), represents a frequency based Reynolds number, and is the ratio of local inertia to viscous terms. These parameters are given by,

$$R = \frac{Uw}{2\nu_f}, \tag{37}$$

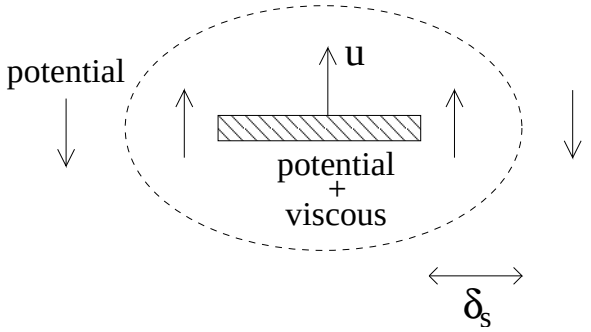

Figure 11: Schematic of the flow around a micron scale cantilever. When the cantilever is moving upward the fluid near the solid no-slip surface moves along with it as a result of viscous drag, an effect that propagates into the fluid at a finite rate. The potential field acts instantaneously throughout the fluid by adapting to the cantilever moving the fluid out of the way, causing fluid far from the cantilever to move in the opposite direction.

$$\beta = \frac{w^2\omega}{4\nu_f}. \tag{38}$$

In the micro scale regime systems commonly undergo high frequency oscillations at very small amplitudes, meaning that $R \ll 1$ and the nonlinear convective inertia term in Eq. (35) can be neglected. However, the local inertia term is still required and $\beta \approx 1$, resulting in the unsteady Stokes equations. Initially the fluid is at rest; all transients that have occured as a result of the force applied in the distant past have dissipated. The motion of the cantilever in fluid is accounted for in the fluid equations by the boundary conditions, where the no slip boundaries have velocities given by the beam equations.

The fluid motion can be decomposed into potential and viscous components [40]. The potential component acts instantaneously. Fluid near the source of the disturbance is pulled along with the body due to viscous drag, Fig 11. This causes a momentum wave to propagate at a finite speed. The interplay between these two components creates complex dynamics in the surrounding fluid. At the micron scale it is possible for the viscous component to affect the

fluid dynamics out to a range that is large compared to the objects themselves. This length can be quantified by the Stokes length,

$$\delta_s = \left(\frac{\nu_f}{\omega_f}\right)^{1/2} = \frac{w}{2}\beta^{-1/2}. \tag{39}$$

The Stokes length approximates the distance over which viscous effects travel during one oscillation of the driving system. For the cantilevers under investigation here $\delta_s \approx 2.5\mu$m. The dynamics of the fluid will be complicated within the range of several stokes lengths and will be investigated further in later chapters.

6 Numerical Simulation Approach

This chapter will describe the numerical simulation approach used to obtain the transient solution to the three dimensional fluid-structure interaction problem. The numerical scheme discussed here has been compared to theory and experiment for validation in [38, 37] for the precise cantilever described in this thesis.

The fluid-structure interaction problem is solved using the CFDRC [12] package with the algorithm discussed in [51]. This algorithm uses a pressure-based method to solve the incompressible Navier-Stokes equations. A finite volume approach is applied to discretize the fluid with first order Euler differencing in time. The finite element method is used to solve the elasticity equations for the solid using the Newmark time integration scheme with parameters for central difference to solve for the transient. The fluid-structure interaction is coupled through the no-slip assumption so that velocity of the fluid and solid mesh are equal at the interfaces. The simulation was assumed to be converged when all residuals had decreased by three orders of magnitude.

Alternative packages for solving the fluid-solid interaction problem are ANSYS [3] and Abaqus [1]. The first step to constructing a useful numerical simulations is determining the size of the domain necessary to eliminate any effects of the bounding walls. Following this the element size and time step used will be discussed.

6.1 Size of the Numerical Domain

The length over which viscous effects act can be quite large for microscale systems. To ensure that the simulation boundaries do not significantly affect the results a series of numerical tests were performed using varying numerical domain sizes. The size of the numerical domain to be used for analysis was

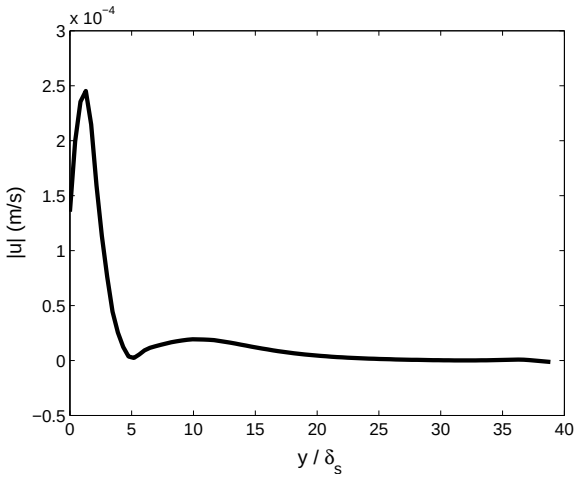

Figure 12: Magnitude of the fluid velocity between the cantilever tip and the side bounding wall (y-direction). See Fig. 10 for coordinate definitions.

chosen such that the magnitude of the fluid velocity went gradually to zero at the walls. Specifically, the distance between the cantilever tip and any numerical bounding wall is chosen such that the velocity field is within 1% of the maximum before reaching the boundary. This means that the effects of the wall will not propagate out into the fluid and change the system dynamics.

Numerical results indicate that the distance from the cantilever tip to the walls should be at least $24\delta_s$ in both y and z, and $12\delta_s$ in x. The numerical domain was chosen to be larger than these constraints in each direction for all numerical simulations presented here. Results from simulations where the numerical domain was smaller than these values yielded cantilever dynamics with lower values of Q and ω_f in agreement with the predicted increase in dissipation for a cantilever oscillating near a wall [25, 16].

6.2 Numerical Parameters

The numerical domain for a single AFM cantilever in fluid has dimensions larger than those described in the previous section. The single cantilever domain

is constructed of $251,328$ elements total, 960 elements in the solid and $250,368$ elements in the fluid. Two cantilever domains have $375,360$ elements, 1920 elements in the solid and $373,440$ elements in the solid. Simulations were run with decreasing element sizes until the variation in the solution was less than 5%. The same grid resolution was used for all single and double cantilever domains. The same number of elements was maintained between the two cantilever tips for $0.1 < s/h < 1$, and the same resolution kept for $s/h = 1$ and $s/h = 2$. Beyond $s/h = 0.1$ the method did not converge as a result of the difference in size between the elements in the solid and in the fluid.

The time step for the single cantilever simulations was 0.2μs and 0.6μs for the multiple cantilever simulations. A single time step takes approximately 15 minutes to run for the single cantilever simulations and 25 minutes for two cantilever simulations on a 3.2 GHz Xeon processor with 4GB of DDR memory. Approximately 700 time steps were necessary to obtain the solution through the point where the fluid can be considered quiescent. In the rest of this paper the deterministic motion of cantilevers in fluid will be quantified using the numerical approach described above.

7 The Stochastic Dynamics of Cantilever Immersed in Viscous Fluid

It is now necessary to obtain a solution to the coupled fluid structure interaction problem given above. An analytical solution exists where the long and thin cantilever has been approximated as an infinite oscillating cylinder [43], an approximation that is valid when $L \gg h$ (see Fig. 10). In this regime the affects of fluid dynamics near the fixed and free ends are negligible and only the flow going around the edges of the beam is considered. The fluid dynamics around each cantilever cross-section is approximated by the flow around an infinite, two dimensional beam with the same cross-section oscillating in the plane. For rectangular geometries with $w \gg h$ this flow field can be modeled by the flow around an infinite oscillating cylinder. In the limit of infinitely thin beams ($h \ll w$) this solution models the fluid effects on a cantilever of rectangular cross-section within 15% in the range of $0.1 \lesssim \beta \lesssim 1000$ [43]. The coupled fluid-structure problem can also be solved using numerical simulations to describe the full three-dimensional flow around a cantilever, including end effects (see [51] for algorithm). The analytical solution will be used to validate the results from simulations of a long thin cantilever in fluid. It will then be possible to use numerical simulations to describe the deterministic dynamics of multiple AFM cantilevers in fluid, such that the stochastic motion can be derived.

7.1 Theory Based on an Infinite Cylinder

The first solutions to the flow around a submersed oscillating cylinder assumed that the system is inviscid, $R \to \infty$ [40]. This assumption is not valid in the regime of interest here where $R \ll 1$, where viscous effects are important. More recently a full solution to the interaction between a very long beam and

a viscous fluid was presented [43]. In this approach the fluid-structure interaction is described by the solution to the unsteady Stokes equations for the flow around an infinite oscillating cylinder. When only the first cantilever mode is modeled the stochastic cantilever motion is described by the Langevin equation in Eq. (9) with the fluid forcing defined as,

$$\hat{F}_f(\omega) = \frac{\pi}{4}\rho_l \omega^2 h^2 \Gamma(\omega)\hat{x}. \tag{40}$$

Here $\Gamma(\omega)$ is the hydrodynamic function obtained by solving the Navier-Stokes equations for an infinite cylinder undergoing transverse oscillations. A solution for the hydrodynamic function has been obtained analytically for the case of beams of circular cross section [40]. In the limits as $\beta \to 0$ and $\beta \to \infty$ the hydrodynamic function for beams of rectangular and circular cross-sections approach the same limit, meaning that a correction to the hydrodynamic function for circular beams can be extrapolated [43]. The correction function is valid within 0.1% in the range of $10^{-6} \lesssim \beta \lesssim 10^4$ [43]. Using this approach it is possible to obtain the damped parameters for the cantilever in fluid directly from the beam geometry and material properties of the fluid and solid. Ref. [43] assumes that the viscous dissipation is frequency independent, an assumption which is not strictly justified. See Ref [38, 37] for a solution including this dependence.

This theory has been compared with experiment for the precise beams considered here [14]. The theory based on an infinite oscillating cylinder predicts a damped frequency $\omega_f = 153 \times 10^3$ rad/s, which is within 4% of the experimental value shown in [14]. The quality number predicted by this theory is $Q = 3.24$, an error of approximately 12% from experiment. A variation in Q of this magnitude does not greatly effect the dynamics of the beams considered. Also, the value presented in [14] may be a typographical error, as numerical simulations

have repeatedly exhibited lower Q values.

7.2 Thermodynamic Approach

The thermodynamic approach for determining the stochastic dynamics of a system from its macroscopic deterministic motion will now be applied to the micron scale cantilevers of interest here. This approach is applicable to physically relevant systems including complex geometries, and has already been applied to a biofunctionalized nanocantilever [20], an array of nanoscale cantilevers [38, 37], V-shaped atomic force microscopes currently in use [2] and the motion of a micron scale cantilever in the presence of a solid wall [17, 25]. The steps followed to apply the fluctuation dissipation theorem to the measurement scheme considered here are:

1. Apply a small step force F_1 in the distant past to one of the cantilevers.
2. Remove the step force at time $t = 0$.
3. Measure the deterministic displacements of the two cantilevers, $X_1(t)$ and $X_2(t)$, until the system returns to a quiescent steady state.
4. Use $X_1(t)$ and $X_2(t)$ to calculate the auto and cross correlations of the equilibrium fluctuations from Eqs. (5) and (6).
5. Use the auto and cross correlations to calculate the noise spectra, $G_{11}(\omega)$ and $G_{12}(\omega)$ from Eqs. (7) and (8).

The deterministic quantities $X_1(t)$ and $X_2(t)$ can be obtained from analytical expressions, numerical simulations, or experiment depending on the complexity of the system under investigation. For the current case a numerical solution using a finite element method [12] for the full transient three dimensional fluid structure interaction will be employed, coupling the Navier-Stokes equations to the equations of elasticity.

7.3 Autocorrelation of a Cantilever in Fluid

Thermally induced oscillations of cantilevers immersed in viscous fluid will be described here using the deterministic deflections obtained from numerical simulations by use of Eq. (5). The autocorrelation of the stochastic cantilever fluctuations is shown in Fig. 13, and is just the scaled macroscopic response. The cantilever modes are not coupled through the fluid and a simple harmonic oscillator is a good fit for the primary mode.

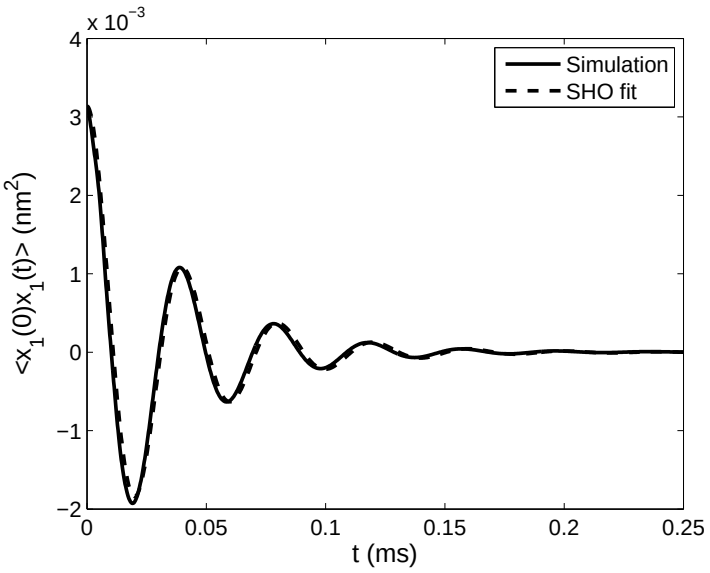

Figure 13: (solid) The autocorrelation of the equilibrium fluctuations in cantilever displacement for a single micron scale cantilever. (dashed) The autocorrelation as fit by a simple harmonic oscillator. Parameters for the fit are given in Table 3.

The effective mass of the cantilever $m_e = 0.243 m_c$ is chosen such that the kinetic energy of an oscillator with all the mass concentrated at the tip is equivalent to that of the cantilever, where $m_c = 2.65 \times 10^{-11}$kg is the mass of the cantilever. Damped parameters for the micron scale cantilever in water as obtained from the simple harmonic oscillator fit are shown in Table 3. For the

m_f/m_e	ω_f/ω_0	γ_f	Q	R	β
8.2	0.35	3.0×10^{-6}kg/s	3.0	39	3.0×10^{-4}

Table 3: Summary of the cantilever response in fluid given by a simple harmonic oscillator model. ω_f and ω_0 are the fundamental frequency in fluid and vacuum, respectively, γ_f is the fluid damping, Q is the quality, and R and β are the Reynolds number and frequency parameter for the cantilever in fluid, respectively.

cantilever being studied this yields a fluid loaded mass of $m_f = 5.26 \times 10^{-11}$kg, which is approximately eight times the effective mass of the cantilever m_e, and a fluid damping of $\gamma_f = 3.0 \times 10^{-6}$kg/s. The fundamental frequency of the cantilever oscillating in fluid is then $\omega_f = (k/m_f)^{1/2} = 160.0 \times 10^3$rad/s (25.5 kHz) and the quality number $Q = m_f\omega_f/\gamma_f = 3.0$. As expected the fundamental frequency for the beam in fluid is smaller than that in vacuum, in this case $\omega_f/\omega_0 = 0.35$. Both the damped oscillation frequency and quality number match reasonably well the values obtained by modeling the cantilever as an infinite oscillating cylinder. The frequency parameter and Reynolds numbers are found to be $\beta = 39.0$ and $R_u = 3.0 \times 10^{-4}$, where the characteristic velocity is chosen to be $\omega_f \langle x^2 \rangle^{1/2}$. As expected $\beta > R$ and $R \ll 1$ indicating that convective inertia is negligible.

The power spectral density for stochastic oscillations of one cantilever immersed in fluid is shown in Fig. 14 along with a simple harmonic oscillator fit of the first cantilever mode. This is the quantity that would be measured in an experimental setup of an atomic force microscope cantilever immersed in water. The response obtained from simulation and the SHO fit differ at very low frequency. This variation at zero frequency does not have any physical relevance. A second peak in the noise spectrum of the full cantilever motion is evident with a magnitude two orders smaller than the first mode. This mode could be

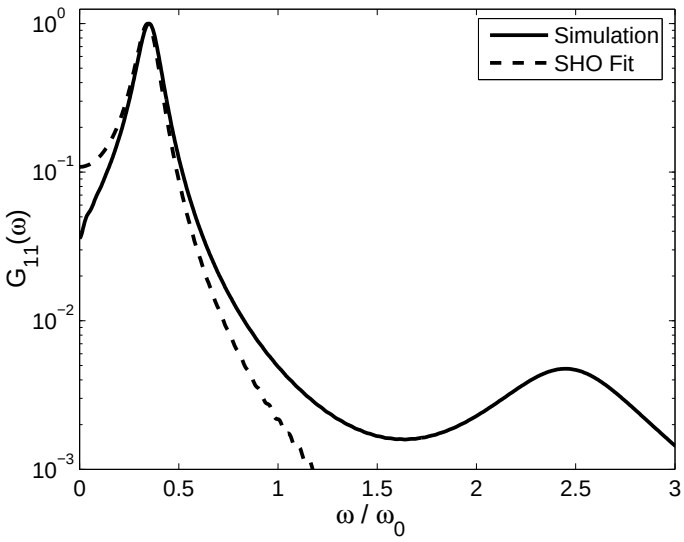

Figure 14: The noise spectrum of thermally induced oscillations, $G_{11}(\omega)$, for a single micron scale cantilever shown with arbitrary units. This is precisely the response that would be obtained from experiment. Also plotted is the noise spectrum for the SHO fit of the first cantilever mode.

modeled as well if necessary.

As required by equipartition of energy, the magnitude of the root mean squared displacement is 3×10^{-3} nm^2, which is the value of the stochastic autocorrelation at $t = 0$. This translates to an average cantilever displacement of $\langle x^2 \rangle^{1/2} = 0.54\mathring{A}$. This value can be used to predict the magnitude of forces exerted as a result of molecules in constant thermal motion,

$$F_{11} = k \left| \langle x_1(0) x_1(t) \rangle \right|_{max}^{1/2} \tag{41}$$

This yields a force sensitivity of $F_{11} = 74$pN, which is the smallest force that can be measured using a single cantilever with this geometry. An estimate of the time resolution possible is given by the time it takes the cantilever to complete an oscillation at its resonant frequency. Using the parameters obtained from the simple harmonic oscillator curve fit for a single cantilever in fluid, this time scale

is estimated to be $\tau \approx 2\pi/\omega_f = 39\mu$s which yields a measurement frequency of 25 kHz. Therefore the cantilever array investigated here can measure forces on the order of 10's of pN with kHz frequency resolution which would make possible the real time measurements of many interesting molecular interactions [39, 5].

The average stochastic motion derived above is equivalent to what would be obtained by averaging over all states of the system. In order to use the latter approach it is necessary to account for all states of the system. This can be accomplished by running the full simulation of the beam in fluid with a random force for a very long time series. Assuming that 1000 periods of oscillation are necessary to fully describe the system, it would take more than 7 months to complete. The next chapter will describe the complex fluid dynamics generated by the oscillation of a microscale cantilever in fluid. It is this motion that will cause the correlated motion in a second beam placed in the fluid.

8 The Flow Field Caused by an Oscillating Cantilever

Now that the physical dynamics of a microscopic cantilever in fluid have been quantified, the stochastic dynamics of the fluid surrounding a micron scale cantilever are of interest. This motion will be described by the deterministic fluid dynamics induced by the macroscopic oscillations of the cantilever. These two are related in the same manner as the deterministic and stochastic cantilever motion; the motion caused by the cantilever as it approaches equilibrium through damped oscillations is directly related to the average flow field caused by stochastic fluctuations. By using the finite element method for a full time dependent three dimensional solution to the fluid structure interaction problem it is possible to obtain information about the fluid flow around a cantilever. The fluid flow will be analyzed in relation to the time at which the cantilever tip has its greatest velocity in the x-direction (maximum in Fig. 16(a)). This corresponds to a cantilever tip velocity of $U_{max} = 2.5\text{mm/s}$ at a time $t^* = 9.0\mu\text{s}$, where $0.22t^*/t_P$ and t_P is the time required for the cantilever to complete its first oscillation. For a simple harmonic oscillator the maximum velocity is expected to occur at one fourth of the period, however the motion is not exactly represented by this fit. The fluid x-direction velocity u in front of the cantilever tip, that is out in the z-direction, is shown for various instances in time in Fig. 16(b), that in the y-direction in Fig. 16(c), and in the x-direction in Fig. 16(d). At $20t^*$ after the initial disturbance the fluid velocity is less than 1% of the maximum and can be considered quiescent.

The velocity in the fluid propagates out as potential and viscous effects, which act instantaneously and at a finite speed, respectively. This interesting interaction will be described in more detail in this section so that the dynamics of a cantilever driven by the induced fluid motion can be better understood. The fluid motion will be shown to have complex dynamics in the range of several

Stokes lengths. These dynamics are discussed in Clark and Paul, 2007 [15].

8.1 Flow Field Around a Cantilever

As expected, the fluid close to the cantilever in y and z moves along with it as a result of viscous drag, while the fluid motion far from the beam is caused primarily by the potential flow field, see Fig. 15, resulting in an opposite sign for fluid velocity far from the cantilever. The behavior of the interaction between the potential field and momentum wave is similar in both y and z, however has different dynamics in x. At the time when the cantilever tip has its greatest velocity the fluid velocity within one Stokes length is in the same direction for both y and z. As the tip begins accelerating, the distance over which the fluid velocity is in the same direction as the tip velocity increases to approximately $3\delta_s$ in the z-direction and $2\delta_s$ in the y-direction at $t/t^* = 2$. This distance reaches a maximum ($\sim 4.5\delta_s$ in z and $\sim 3.5\delta_s$ in the y) as the tip velocity approaches zero. When the tip velocity crosses zero the fluid velocity becomes out of phase with the tip velocity everywhere and the distance begins growing again, as seen at $t/t^* = 2.5$. As the cantilever slows down there is more time for viscous effects to propagate into the fluid and the fluid returns to a state similar to that at $t/t^* = 1$. The difference in the maximum over which the viscous component has a large effect means that the Stokes layer is larger in z than in y so objects can be placed closer to the side of a cantilever than in front of the tip before encountering viscous dominated flow. Also, the velocity in y-direction dissipates at a faster rate than that in the z, such that objects beside a cantilever will experience hydrodynamic forcing to a lesser degree than something in front of the tip. The fluid velocity in the x-direction is positively in phase with the tip for most times at large distances from the cantilever, see Fig. 16(d). Unlike in the other two directions, in this region of the fluid the potential flow is always in

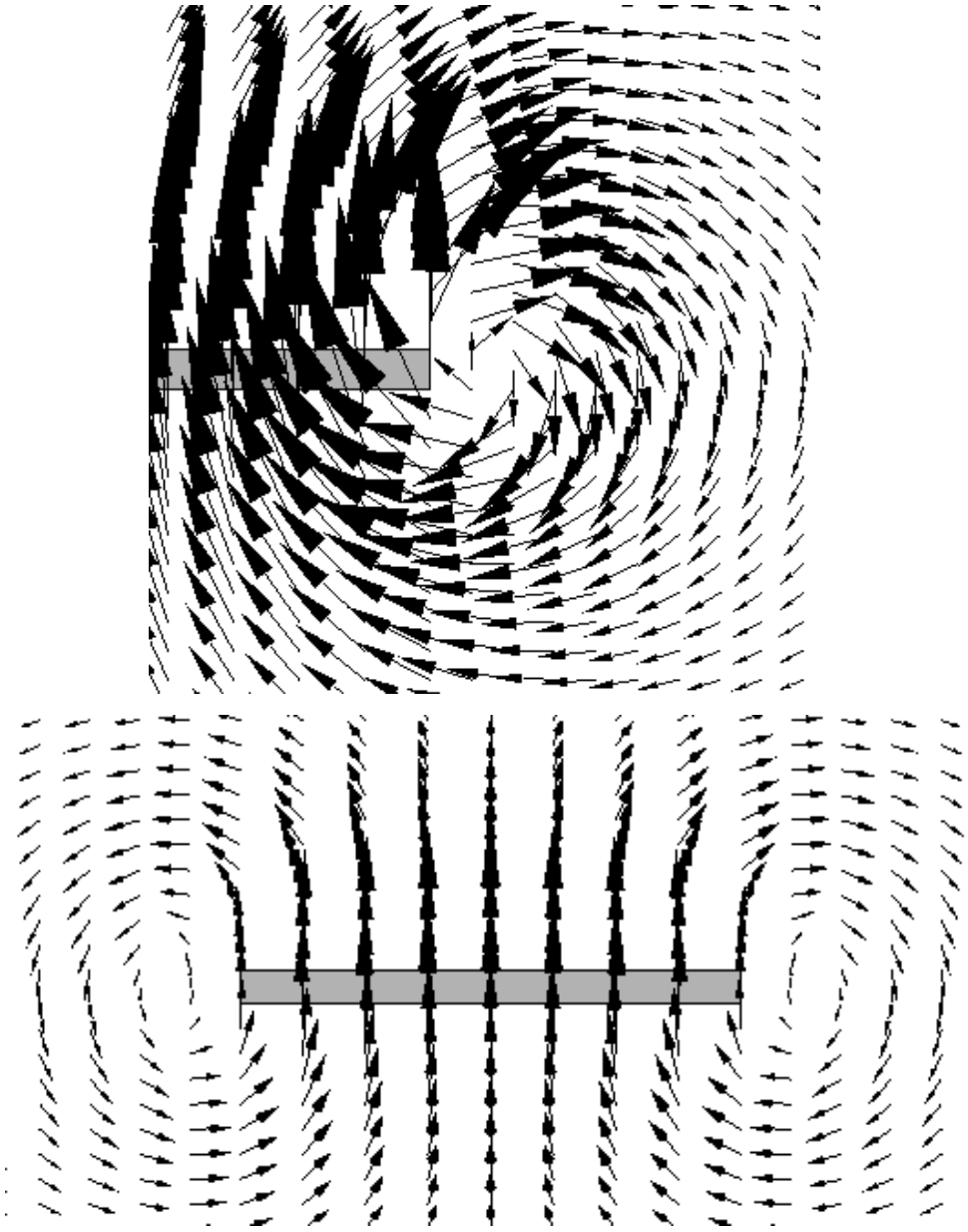

Figure 15: The three-dimensional flow field near the tip (distal end) of an oscillating atomic force microscope. The flow field is a snap shot in time at the instant where the cantilever is at its maximum velocity, $t^* = 9.0\mu$s. (top) Flow field over the cantilever tip in the the $x - z$ plane. The base of the cantilever is to the far left of the figure and is not shown. (bottom) Flow field around the sides of the cantilever in the $x - y$ plane. See Fig. 10 for coordinate axis definitions. In both figures the largest arrow indicates a fluid velocity of $U = 2.5$ mm/s.

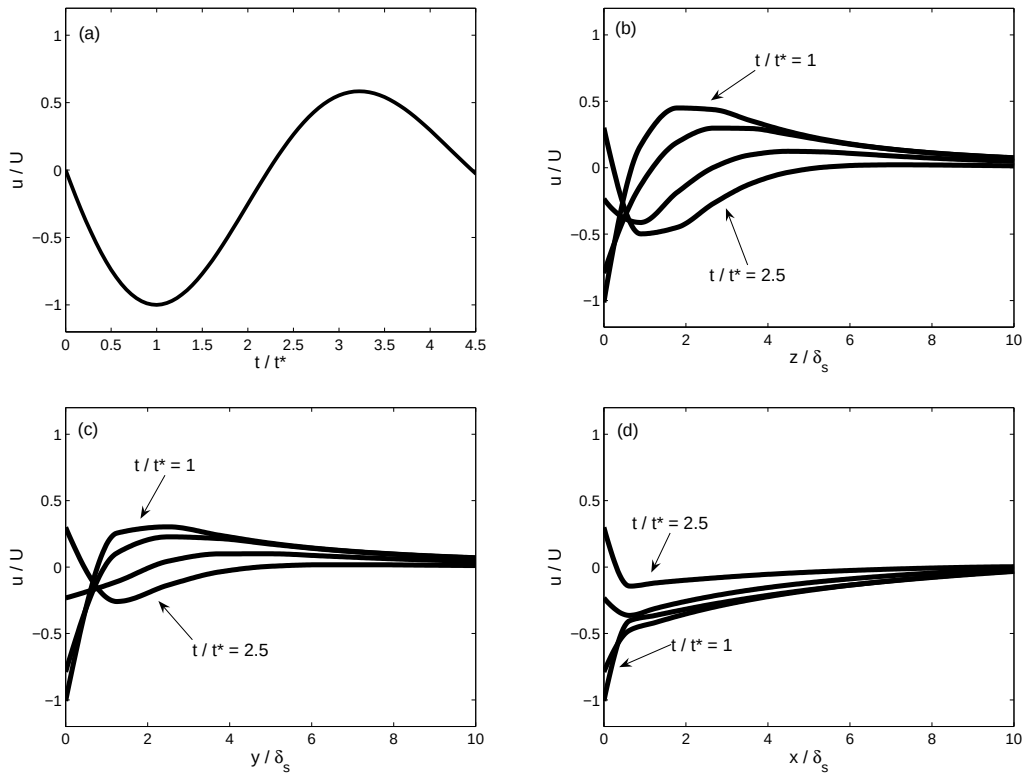

Figure 16: (a) The cantilever tip velocity as a function of time. After $20t^*$ the tip velocity is within 1% of the maximum value. (b) The variation in the x-component of the fluid velocity u as a function of distance in the z-direction measured from the tip of the cantilever at various times during the cantilevers oscillations. (c) The variation in the x-component of the fluid velocity u as a function of distance in the z-direction measured from the tip of the cantilever at various times during the cantilevers oscillations. (d) The variation in the x-component of the fluid velocity u as a function of distance in the x-direction measured from the tip of the cantilever at various times during the cantilevers oscillations. In each plot curves are shown for $t/t^* = 1, 1.5, 2, 2.5$, where $t/t^* = 1$ and 2.5 are labeled and the other two are in sequence.

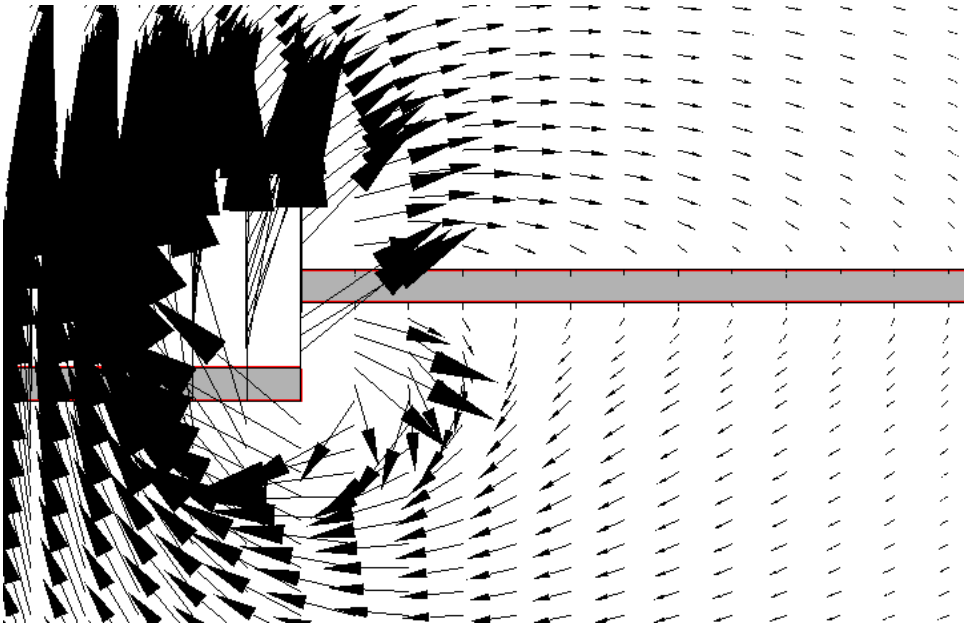

Figure 17: A zoomed in view of the flow field around two cantilevers in the opposing configuration investigated here for the $x-z$ plane. This figure focuses on the adjustment of the flow field to the presence of a second cantilever. The largest arrow corresponds to U_{max}

the same direction as the cantilever velocity. As the velocity crosses zero there is a region where the fluid velocity is out of phase with the cantilever between two in phase regions. At later times when viscous effects have diffused into the fluid, the velocity is again in phase everywhere.

When a second cantilever is placed within the Stokes layer of the first cantilever the flow field becomes more complex. This can cause the formation of complicated flow patterns as the two move relative to each other, Fig. 17. A description of the dynamics that cause this flow is necessary to understand fully the hydrodynamic coupling between micron sized objects in fluid.

9 Fluid Coupled Cantilever Arrays

The previous chapters of this thesis quantified the stochastic dynamics of a microscale cantilever and the surrounding fluid. The same thermodynamic approach will now be used to quantify the stochastic dynamics of an array of microscale cantilevers immersed in viscous fluid. The Brownian force experienced by neighboring cantilevers in fluid will be uncorrelated. In the absence of a biomolecule tethered between the cantilever tips only the coupling due to hydrodynamic forcing induced by the motion of a cantilever will be present. In order to describe the coupled stochastic motion of multiple cantilevers in fluid, the fluctuation-dissipation theorem will be applied to the deterministic dynamics of two microscale cantilevers (see [15]). In the absence of an analytical solution for multiple cantilevers coupled by a hydrodynamic interaction, numerical simulations will be used to obtain the full three dimensional transient solution.

9.1 Two AFM Cantilevers in Fluid

The finite element method is used to describe the deterministic motion of two micron scale cantilevers coupled by fluid motion in the orientation shown in Fig. 10. This orientation is chosen in order to minimize the fluid coupling while also maximizing the effect the cantilever fluctuations have on a tethered protein. It is found that the presence of a second cantilever does not have an appreciable effect on the beam autocorrelation function. The cross-correlation of thermal oscillations for a cantilever forced into motion by the fluid dynamics induced by the presence of another cantilever undergoing stochastic fluctuations is shown in Fig. 18(b) for a range of separations. As expected the dissipative effects in the fluid cause the magnitude of the cross-correlation to decrease as the separation increases.

The auto and cross-correlation for two beams separated by $s/h = 0.1$ are plotted in Fig. 18(a) to emphasize the phase shift between the deflections. At each time when the autocorrelation crosses zero there is a peak in the cross-correlation, meaning that the two are out of phase by approximately one fourth of a period. This is the point in each oscillation at which the autocorrelation has its greatest velocity. The dynamics of the cross-correlation for very short times are a result of the potential part of the velocity field, and as a result cross-correlation increases when the autocorrelation begins decreasing.

The minimum cantilever separation investigated here ($s = 200nm$) is a result of computational constraints given by the numerical method used. The actual separation between two micron scale cantilevers in an experimental setup to measure the dynamics of single molecules will be dependent upon the size of the probes used on each cantilever [23] and the method used to tether the molecule [4, 46]. For the readily available cantilever tips and adsorbtion techniques, the range of separations explored here spans what would be expected in experiment [33, 4].

The cross-correlation of the equilibrium fluctuations can be used to describe the magnitude of hydrodynamic coupling for the setup of interest. The maximum value of the cross-correlation can be used to find the magnitude of fluid forcing caused by the cantilever motion and the height of the oscillations induced. From Fig. 18(b) for the case with the closest separation, $s/h = 0.1$, the maximum magnitude of the cross-correlation $|\langle x_1(0)x_2(t)\rangle|_{max} \approx 2.9 \times 10^{-4}\text{nm}^2$ which yields a root mean squared displacement of $0.17\mathring{A}$. The spectral density of the equilibrium fluctuations is shown in Fig. 19 as a function of frequency and cantilever separation. This is the power spectrum that would be measured in an experimental setup with each separation. There is a shift in the spectral properties to lower frequencies as the separation increases. This lag associated

with larger separations is indicative of viscous effects propagating outward at a finite rate. It is also interesting that there is a frequency, ω^*, at which the dynamics of the two cantilevers will be uncorrelated, that is $G_{12}(\omega^*) = 0$. It may be possible to take advantage of this to derive an experimental scheme that minimizes the fluid coupling, allowing for greatly improved measurement resolution. The variation of this frequency with separation is shown in Fig. 20 along with a linear curve fit given by,

$$\omega^*/\omega_0 = -1.32 \times 10^{-2}(s/h) + 0.401. \tag{42}$$

The error in this fit is $\eta_E = 0.2\%$ using the definition,

$$\eta_E = \frac{\sqrt{\sum_{s/h} \left(\omega^*(s/h) - \bar{\omega^*}(s/h)\right)^2}}{\sqrt{\sum_{s/h} \left(\omega^*(s/h)\right)^2}}. \tag{43}$$

Here $\bar{\omega^*}(s/h)$ is the value of ω^* predicted by the curve fit at s/h.

9.2 Force Resolution Improvement

An estimate of the force resolution for the measurement scheme under investigation can be obtained from the maximum magnitude of the cross-correlation of equilibrium fluctuations,

$$F_{12} = k \left| \langle x_1(0) x_2(t) \rangle \right|_{max}^{1/2}. \tag{44}$$

For the case of $s/h = 0.1$ the value of the force sensitivity is calculated to be approximately 22pN, a improvement of more than three fold over the resolution attainable with a single micron scale cantilever, $F_{11} = 74$pN. This means that the dynamics of a molecule with magnitudes as small as 22pN can be measured by tethering it between two cantilevers separated by 200nm. This is a very important regime; for example the forces exerted by the protein lysozyme as it

undergoes conformational changes are on the order of 50pN [39]. The trend of force sensitivity versus separation is shown in Fig. 21 along with a quadratic curve fit given by,

$$F_{12}/F_{11} = -7.3 \times 10^{-3}(s/h)^2 - 1.33 \times 10^{-2}(s/h) + 0.3059. \tag{45}$$

This fit has an error of $\eta_E = 0.4\%$ using Eq. (43). For the range of separations investigated here the force sensitivity improves between three and four fold. The gradual improvement in force sensitivity with increasing separation shows that the correlated measurement scheme discussed is useful for the range of separations expected for single molecule experiments.

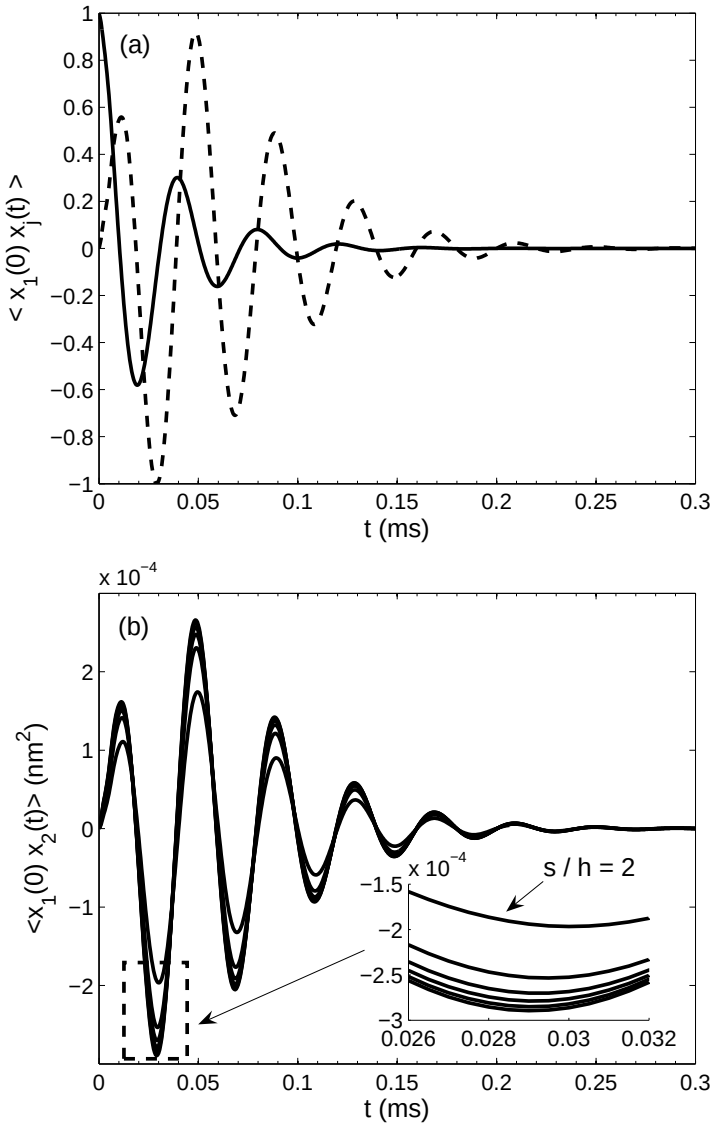

Figure 18: (a) The auto (solid line) and cross-correlation (dashed line) are plotted to emphasize the phase difference. The two functions have been normalized using $3 \times 10^{-3}\text{nm}^2$ for the autocorrelation and $2.9 \times 10^{-4}\text{nm}^2$ for the cross-correlation. (b) The cross-correlation of the equilibrium fluctuations in cantilever displacement over the range of cantilever separations $s/h = 0.1, 0.3, 0.5, 0.7, 1, 2$. (inset) A detailed view of the peak with the maximum magnitude showing a decrease in magnitude with separation.

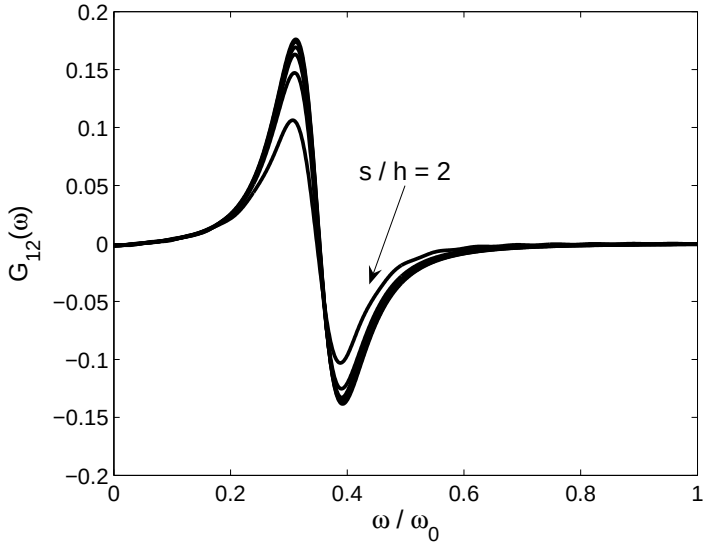

Figure 19: The noise spectrum $G_{12}(\omega)$ for the cantilever array shown with arbitrary units. Results are shown for cantilever separations of $s/h = 0.1, 0.3, 0.5, 0.7, 1, 2$ and normalized by the same factor as $G_{11}(\omega)$ in Fig. 10.

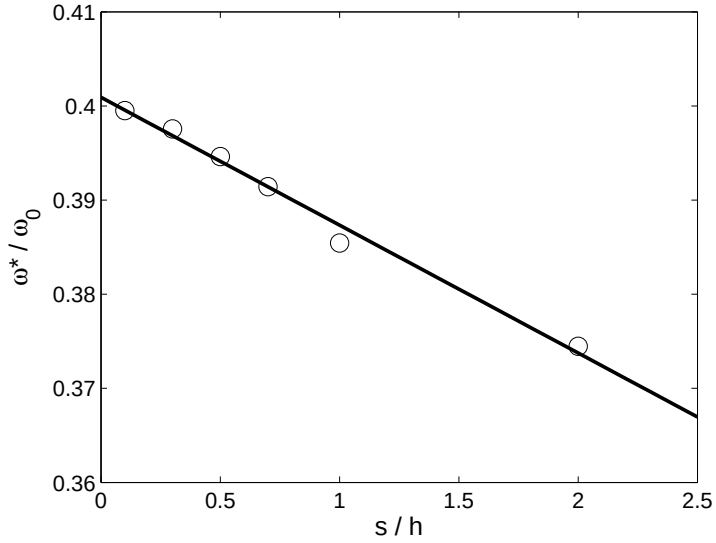

Figure 20: The frequency at which the spectral crosses as a function of separation. The line is a linear curve fit given by $\omega^*/\omega_0 = -1.32 \times 10^{-2}(s/h) + 0.401$.

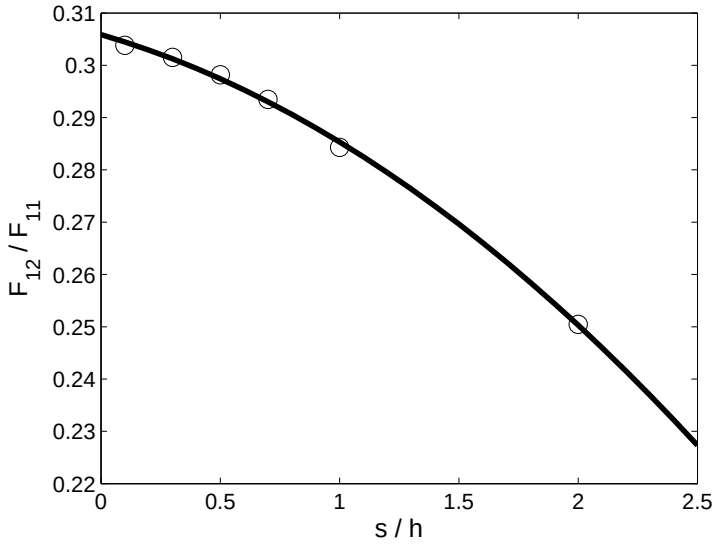

Figure 21: Force sensitivity as a function of beam separation. Forces have been normalized by the magnitude of stochastic forcing on a single AFM cantilever ($F_{11} = 74$ pN). A quadratic curve fit has also been plotted with equation $F_{12}/F_{11} = -7.3 \times 10^{-3}(s/h)^2 - 1.33 \times 10^{-2}(s/h) + 0.3059$.

10 Conclusions

This thesis described the random fluctuations experienced by microscopic systems. The average stochastic dynamics of a simple system are derived from the deterministic motion of the system as it returns to equilibrium by application of the fluctuation-dissipation theorem. This method is then extended to derive the dynamics of a microscopic cantilever immersed in viscous fluid from numerical simulations. Finally, the fluctuation-dissipation theorem is used to quantify the stochastic dynamics of an array of two AFM cantilevers coupled by fluid motion for the purpose of investigating single molecules. By measuring correlations between the random fluctuations in cantilever displacements it is possible to lower the noise floor inherent in physical systems. It is found that the force sensitivity of a single cantilever can be improved by 3 to 4 fold by using correlated measurements of two cantilevers with separations over the range investigated here. This thesis reveals that by using correlated measurements it is possible to investigate the dynamics of single molecules undergoing conformational changes in real time.

The dynamics of the fluid surrounding an oscillating cantilever are also quantified. The complex flow field around the tip of the cantilever suggests that the configuration of the cantilever array is an important determining factor in the resulting cantilever correlations. The cantilever orientation discussed here is chosen in an attempt to minimize the correlation due to hydrodynamic effects, while maximizing the effect the cantilever motion has on the tethered biomolecule. Also interesting is that the power spectrum of cross-correlations in stochastic fluctuations is zero at a particular frequency. Because of the minimized correlation in the frequency band surrounding this crossing, it may be possible to exploit this fact to minimize the correlations and therefore improve the force sensitivity in experiments by performing measurements in this band.

The approach used here to quantify the stochastic dynamics of physical systems is quite general and can be extended to include more complex geometries and array configurations that are motivated by experiment. This technique can be extended to model more experimentally realistic physical setups in order to more accurately predict the characteristics of proposed measurement methods. Theoretical calculations, such as these, will provide important insight necessary for the interpretation and design of future micro and nanoscale technologies that exploit inherent thermal fluctuations.

List of References

[1] Abaqus, Inc. www.abaqus.com.

[2] T. R Albrecht and C. F. Quate. Atomic resolution imaging of a nonconductor by atomic force microscopy. *J. Appl. Phys*, 62(7):2599–2602, 1987.

[3] ANSYS, Inc. www.ansys.com.

[4] J. L. Arlett, M. R. Paul, J. Solomon, M. C. Cross, S. E. Fraser, and M. L. Roukes. Nanomechanical devices for single-molecule biophysics. In *Controlled Nanoscale Motion in Biological and Artificial Systems*, Nobel Symposium 131. Springer-Verlag, 2005.

[5] G. Bao and S. Suresh. Cell and molecular mechanics of biological materials. *Nature Materials*, 2:715–725, 2003.

[6] G Binnig, C. F. Quate, and Ch. Gerber. Atomic force microscope. *Phys. Rev. Lett.*, 56(9):930–933, 1986.

[7] C. Bustamante, J. Macosko, and G. Wuite. Grabbing the cat by the tail: manipulating molecules one by one. *Nature Reviews*, 1:130–136, 2000.

[8] H.-J. Butt and M. Jaschke. Calculation of thermal noise in atomic force microscopy. *Nanotech.*, 6:1–7, 1995.

[9] H. B. Callen and R. F. Greene. On a theorem of irreversible thermodynamics. *Phys. Rev.*, 86(5):702–710, 1952.

[10] H. B. Callen and A. T. Welton. Irreversibility and generalized noise. *Phys. Rev. Lett.*, 83(1):34–40, 1951.

[11] R. Car and M. Parrinello. Unified approach for molecular-dynamics and density-functional theory. *Phys. Rev. Lett.*, 55(22):2471–2474, 1985.

[12] CFD Research Corporation, 215 Wynn Dr. Huntsville AL 35805.

[13] D. Chandler. *Introduction to Modern Statistical Mechanics.* Oxford University, Press, 1987.

[14] J. W. M. Chon, Mulvaney P., and J. E. Sader. Experimental validation of theoretical models for the frequency response of atomic force microscope cantilever beams immersed in fluids. *J. Appl. Phys.*, 87(8):3978–3988, 2000.

[15] M.C. Clark and M.R. Paul. The stochastic dynamics of an array of atomic force microscopes in viscous fluid. *Nanotech., submitted*, 2006.

[16] R. J. Clarke, S. M. Cox, P. M. Williams, and O. E. Jensen. The drag on a microcantilever oscillating near a wall. *J. Fluid Mech.*, 545:397–426, 2005.

[17] R. J. Clarke, O.E. Jensen, J. Billingham, A.P. Pearson, and P.M. Williams. Stochastic elastohydrodynamics of a microcantilever oscillating near a wall. *Phys. Rev. Lett.*, 96(5):050801, 2006.

[18] J.P. Cleveland, S. Manne, D. Bocek, and Hansma P.K. A nondestructive method for determining the spring constant of cantilevers for scanning force microscopy. *Rev. Sci. Instrum.*, 64(2):403–405, 1993.

[19] H. Craighead. Nanoelectromechanical systems. *Science*, 290:1532–1535, 2000.

[20] J. Dorignac, A Kalinowski, S. Erramilli, and P. Mohanty. Dynamical response of nanomechanical oscillators in immiscible viscous fluid for in vitro biomolecular recognition. *Phys. Rev. Lett.*, 96:186105, 2006.

[21] R. Erlandsson, G.M. McClellan, C.M. Mate, and S. Chiang. Atomic force microscopy using optical interferometry. *J. Vac. Sci.*, 6(2):266–270, 1988.

[22] R.P. Feynman. There's plenty of room at the bottom. *Engineering and Science, Caltech*, 1960.

[23] R. Garcia and R. Perez. Dynamic atomic force microscopy methods. *Surf. Sci. Rep.*, pages 197–301, 2002.

[24] F. J. Giessibl. Advances in atomic force microscopy. *Rev. Mod. Phys.*, 75:949–983, 2003.

[25] C. P. Green and J. E. Sader. Small amplitude oscillations of a thin beam immersed in a viscous fluid near a solid surface. *Phys. Fluids*, 17:073102, 2005.

[26] G. Karniadakis, A. Beskok, and N. Aluru. *Micro flows*. Springer, 2001.

[27] L. D. Landau and E. M. Lifshitz. *Theory of elasticity*. Butterworth-Heinemann, 1959.

[28] H.L. Ma, J. Jimenez, and R. Rajagopalan. Brownian fluctuation spectroscopy using atomic force microscopes. *J. Appl. Phys.*, 61:4723–4729, 1987.

[29] Y. Martin, C. C. Williams, and H. K. Wickramasinghe. Atomic force microscope force mapping and profiling on a sub 100-$\AA$ scale. *J. Appl. Phys.*, 61:4723–4729, 1987.

[30] Mathematica, Wolfram Research. www.wolfram.com.

[31] J. C. Meiners and S. R. Quake. Direct measurement of hydrodynamic cross correlations between two particles in an external potential. *Phys. Rev. Lett.*, 82(10):2211–2214, 1998.

[32] J. C. Meiners and S. R. Quake. Femtonewton force spectrroscopy of single extended dna molecules. *Phys. Rev. Lett.*, 84(21):5014–5017, 2000.

[33] NanoScience Instruments, store.nanoscience.com.

[34] Olympus, http://www.olympus.co.jp/en/insg/probe/en/specsisoftE.html.

[35] L. Onsager. Reciprocal relations in irreversible processes. II. *Phys. Rev.*, 38:2265–2279, 1931.

[36] R. L. Panton. *Incompressible fluid flow*. Wiley, 2005.

[37] M. R. Paul, M.T. Clark, and M. C. Cross. Stochastic dynamics of micron and nanoscale elastic cantilevers in fluid: fluctuations from dissipation. *Nanotech., submitted*, 2006.

[38] M. R. Paul and M. C. Cross. Stochastic dynamics of nanoscale mechanical oscillators immersed in a viscous fluid. *Phys. Rev. Lett.*, 92(23):235501, 2004.

[39] M. Radmacher, M. Fritz, H. Hansma, and P. K. Hansma. Direct observation of enzymatic activity with the atomic force microscope. *Science*, 265:1577–1579, 1994.

[40] L. Rosenhead. *Laminar Boundary Layers*. Clarendon, Oxford, 1963.

[41] M. L. Roukes. Nanoelectromechanical systems. condmat/0008187, 2000.

[42] M. L. Roukes. Personal communication, 2006.

[43] J. E. Sader. Frequency response of cantilever beams immersed in viscous fluids with applications to the atomic force microscope. *J. Appl. Phys.*, 84(1):64–76, 1998.

[44] S. A. Schaaf and P. L. Chambre. *Flow of rarefied gases*. Princeton University Press, 1961.

[45] S.B. Smith, L. Finzi, and C. Bustamante. Direct mechanical measurements of the elasticity of single dna molecules by using magnetic beads. *Science*, 285:1122–1126, 1992.

[46] J.E. Solomon and M.R. Paul. The kinetics of analyte capture on nanoscale sensors. *Biophys J.*, 90:1842–1852, 2006.

[47] T.R. Strick, J.F. Allemand, D. Bensimon, A. Bensimon, and V. Croquette. The elasticity of a single supercoiled dna molecule. *Science*, 271:1835–1837, 1996.

[48] K. Svoboda, C.F. Schmidt, B.J. Schnapp, and S.M. Block. Direct observation of kinesin stepping by optical trapping interferometry. *Nature*, 365:721–727, 1993.

[49] M. B. Viani, T. E. Schaffer, and A. Chand. Small cantilevers for force spectroscopy of single molecules. *J. Appl. Phys.*, 86(5):2258–2262, 1999.

[50] Wikipedia online encyclopedia, Atomic packing factor. en.wikipedia.org.

[51] H. Q. Yang and V. B Makhijani. A strongly-coupled pressure-based CFD algorithm for fluid-structure interaction. *AIAA-94-0179*, pages 1–10, 1994.